NASA/CR—2005-213646

# Parametric Analyses of Potential Effects on Upper Tropospheric/Lower Stratospheric Ozone Chemistry by a Future Fleet of High Speed Civil Transport (HSCT) Type Aircraft

Mayurakshi Dutta, Kenneth O. Patten, and Donald J. Wuebbles
University of Illinois at Urbana-Champaign, Champaign, Illinois

June 2005

## The NASA STI Program Office . . . in Profile

Since its founding, NASA has been dedicated to the advancement of aeronautics and space science. The NASA Scientific and Technical Information (STI) Program Office plays a key part in helping NASA maintain this important role.

The NASA STI Program Office is operated by Langley Research Center, the Lead Center for NASA's scientific and technical information. The NASA STI Program Office provides access to the NASA STI Database, the largest collection of aeronautical and space science STI in the world. The Program Office is also NASA's institutional mechanism for disseminating the results of its research and development activities. These results are published by NASA in the NASA STI Report Series, which includes the following report types:

- TECHNICAL PUBLICATION. Reports of completed research or a major significant phase of research that present the results of NASA programs and include extensive data or theoretical analysis. Includes compilations of significant scientific and technical data and information deemed to be of continuing reference value. NASA's counterpart of peer-reviewed formal professional papers but has less stringent limitations on manuscript length and extent of graphic presentations.

- TECHNICAL MEMORANDUM. Scientific and technical findings that are preliminary or of specialized interest, e.g., quick release reports, working papers, and bibliographies that contain minimal annotation. Does not contain extensive analysis.

- CONTRACTOR REPORT. Scientific and technical findings by NASA-sponsored contractors and grantees.

- CONFERENCE PUBLICATION. Collected papers from scientific and technical conferences, symposia, seminars, or other meetings sponsored or cosponsored by NASA.

- SPECIAL PUBLICATION. Scientific, technical, or historical information from NASA programs, projects, and missions, often concerned with subjects having substantial public interest.

- TECHNICAL TRANSLATION. English-language translations of foreign scientific and technical material pertinent to NASA's mission.

Specialized services that complement the STI Program Office's diverse offerings include creating custom thesauri, building customized databases, organizing and publishing research results . . . even providing videos.

For more information about the NASA STI Program Office, see the following:

- Access the NASA STI Program Home Page at ***http://www.sti.nasa.gov***

- E-mail your question via the Internet to help@sti.nasa.gov

- Fax your question to the NASA Access Help Desk at 301–621–0134

- Telephone the NASA Access Help Desk at 301–621–0390

- Write to:
  NASA Access Help Desk
  NASA Center for AeroSpace Information
  7121 Standard Drive
  Hanover, MD 21076

NASA/CR—2005-213646

# Parametric Analyses of Potential Effects on Upper Tropospheric/Lower Stratospheric Ozone Chemistry by a Future Fleet of High Speed Civil Transport (HSCT) Type Aircraft

Mayurakshi Dutta, Kenneth O. Patten, and Donald J. Wuebbles
University of Illinois at Urbana-Champaign, Champaign, Illinois

Prepared under Contract NAS3–03091

National Aeronautics and
Space Administration

Glenn Research Center

June 2005

## Acknowledgments

This research was supported in part by The Boeing Company. We thank Daniel Youn, School of Earth and Environmental Sciences, Seoul National University, for his help with the upgradation of the UIUC-2D model dynamics and comparison of model results with observation data.

This report contains preliminary findings, subject to revision as analysis proceeds.

Available from

NASA Center for Aerospace Information
7121 Standard Drive
Hanover, MD 21076

National Technical Information Service
5285 Port Royal Road
Springfield, VA 22100

Available electronically at http://gltrs.grc.nasa.gov

# Parametric Analyses of Potential Effects on Upper Tropospheric/ Lower Stratospheric Ozone Chemistry by a Future Fleet of High Speed Civil Transport (HSCT) Type Aircraft

Mayurakshi Dutta, Kenneth O. Patten, and Donald J. Wuebbles
University of Illinois at Urbana-Champaign
Department of Atmospheric Sciences
Urbana, Illinois 61801

## 1. Introduction

Although no such aircraft is currently under development, there has been much consideration over the last decade of the potential impacts on the environment of projected fleets of supersonic passenger jets that would fly approximately 300 passengers at roughly twice the speed of sound. These High Speed Civil Transport (HSCT) aircraft are likely to be reconsidered in the future if it is thought that various engineering and fuel use concerns can be resolved. Thus, evaluation of the potential effects of such aircraft on the global environment remains valuable. In particular, it should be noted that existing ozone-impact studies have not fully analyzed the potential extent of possible flight and emissions criteria for such aircraft.

The IPCC evaluated the effect of supersonic engine effluent on stratospheric ozone ($O_3$) using two-dimensional (2–D) and three-dimensional (3–D) chemical transport models (CTMs) of the global atmosphere in the 1999 IPCC aircraft assessment (IPCC, 1999). An earlier version of our 2–D model, submitted by colleagues at Lawrence Livermore National Laboratory, was included in the assessment. Since the aircraft do not match any specific design, the IPCC report treated the study of supersonic aircraft in a parametric way looking at more than 50 scenarios. We chose seven scenarios from that list for assessing the current version of the UIUC zonally-averaged 2–D model of the global atmosphere in terms of the potential atmospheric impact on stratospheric ozone from assumed fleets of HSCT aircraft. This version of the model has been used for the subsequent studies in this report.

In this study, we will focus on the type of HSCT considered over the last decade, where, because of noise concerns, the aircraft is primarily allowed to fly at supersonic speeds only over the oceans. Like other aircraft based on current jet engine technology, these HSCT type aircraft will emit nitrogen oxides ($NO_x = NO + NO_2$), carbon dioxide ($CO_2$), water vapor ($H_2O$) and sulfur, the latter if it is still in the fuel. In the studies of ozone effects presented here, only $NO_x$ and $H_2O$ emissions are considered. Although there would also be some emissions of hydrocarbons and carbon monoxide, past studies indicate that these emissions are unlikely to be important in the global atmosphere.

This report analyzes the potential impact of projected fleets of HSCT aircraft through a series of parametric analyzes that examine the envelop of potential effects on ozone over a range of total fuel burns, emission indices of nitrogen oxides [E.I. ($NO_x$)], and cruise altitudes.

## 2. Methodology

### 2.1 Description of Scenarios

***2.1.1 Scenarios for comparison with IPCC (1999)***.—The seven scenarios chosen for comparing our 2–D model with the IPCC (1999) assessment are S1b, S1c, S1d, S1e, S1i, S1k, and S9h (table 3). These supersonic aircraft scenarios for 500 or 1000 HSCT aircraft would cruise at standard height (approximately 18 to 21 km altitude range). The HSCT scenarios contain subsonic aircraft as well as HSCT commercial aircraft, with the combination accounting for the same passenger demand as in the

baseline subsonic only scenario for 2015 or 2050. The HSCT scenarios are analyzed relative to the corresponding 2015 or 2050 baseline scenario.

In all these scenarios the reference atmosphere is consistent with a sulfate area density (SAD) corresponding to a background atmosphere, labeled SA0, without major input from volcanic eruptions or from aircraft. For the scenarios S1k and S9h a sulfur dioxide gas to particle conversion factor of 10 percent is used in the perturbation case. Boundary conditions for the background atmosphere for long-lived gases are changed to 2015 concentrations for all the scenarios except S9h for which a 2050 background was used as given in table 1. For the S9h scenario the background $NO_x$ is increased by a factor of 129 percent and the carbon monoxide (CO) is increased by 87 percent based on tables 4 to 2 of IPCC (1999); these values are then used in deriving the background steady state concentrations.

***21.2 HSCT Type Scenarios***.—A set of emissions scenarios for HSCT type aircraft have been developed for the Ultra-Efficient Engine Technology (UEET) Program at the NASA Glenn Research Center by Baughcum et al. (2002). These scenarios consider a range of possible design criteria for a fleet of 500 HSCT aircraft. The particular variables chosen for the parametric studies to evaluate the atmospheric effects of this type of aircraft are fuel burn, cruise altitude, and emission index of $NO_x$. From fuel burn, one can readily determine the emissions of water vapor (and carbon dioxide and several other types of emissions).

Fuel sulfur content was not considered in this parametric study for two reasons. The primary concerns about sulfur emissions on ozone occur if there is rapid conversion of the sulfur into sulfate aerosols within the aircraft plume, before the emissions are well mixed into the background atmosphere. However, recent studies suggest less than 5 percent of the sulfur emissions are likely to be converted in the plume. If so, such emissions are likely to have a negligible effect on the derived changes in ozone. Also, it is generally thought that sulfur will be eliminated from the fuel over the next few decades.

Baughcum et al. also developed a scenario for the subsonic commercial aircraft flights by airplane types, along with corresponding emissions projected for 2020. Flight traffic for the projected fleet of 500 HSCT aircraft then displaces part of the subsonic projection. As mentioned earlier, for the HSCT scenarios developed, it was assumed that no supersonic flights would be allowed over land (any flights over land by HSCT aircraft would need to be at subsonic speeds). The total cruise fuel used for this type of HSCT was chosen to be reasonably represented by assuming it would be equivalent to the fuel use represented by 10 to 20 percent of the total cruise fuel use for flights greater than 2500 nautical miles. This corresponds to fuel burn of 73 to 146 million pounds per day. These two fuel use values were used for differing scenarios.

The emission index of $NO_x$ is an important issue since much of the concern regarding the atmospheric effects of aircraft emissions arises from $NO_x$ emissions. For this study, emission indices of 5, 10, and 20 g/kg of fuel were considered for the two fuel burn cases, which span the range of current and projected engine technology.

Four two kilometer altitude bands ranging from 13 to 21 km (representation of these in our model is in log pressure altitude) were chosen for evaluating the effect of cruise altitudes on ozone concentrations so that emissions were put into the bands of 13 to 15, 15 to 17, 17 to 19, and 19 to 21 km. This range is broader than actually expected for the cruise altitude of HSCT aircraft, but in our study we also wanted to extend the range to consider the full range of effects on ozone.

Since the 2–D model uses a grid based on pressure coordinates with 1.5 km between zones, the emissions were spread across two model layers of the model. The pressure grid of the emissions was remapped onto our pressure grid. Also, after zonally averaging, the emission file was remapped from its 1° latitude distribution onto the 5° latitude resolution of the model.

In the model, the background atmosphere was set to a 2020 atmosphere with the source gas concentrations of the long-lived species changed according to table 1. This choice of background concentrations of long-lived constituents is based on the A2 scenario recommended in IPCC (Houghton et al., 2001). Scenario A2 is in the upper middle of the range of scenarios being used for analyzing the potential effects of human activities on climate. The scenarios were analyzed relative to the

corresponding 2020 base with a subsonic aircraft included based on the 2020 subsonic aircraft emissions developed by Baughcum et al. (2002). The HSCT type scenarios, which also contain the revised subsonic emissions resulting from including the HSCT fleet, were then evaluated for their effects on ozone relative to this background atmosphere.

TABLE 1.—BACKGROUND SURFACE CONCENTRATIONS FOR LONG-LIVED GASES IN 2015 FROM IPCC (1999) AND IN 2020 BASED ON SCENARIO A2 IN IPCC (2001)

| Chemical Species | 2015 | 2020 | 2050 |
|---|---|---|---|
| CFC–11 (pptv) | 220 | 214 | 120 |
| CFC–12 (pptv) | 470 | 486 | 350 |
| CFC–13 (pptv) | 80 | 72 | 60 |
| CC14 (pptv) | 70 | 59 | 35 |
| HCFC–22 (pptv) | 250 | 229 | 15 |
| $CH_3CC1_3$ (pptv) | 3 | 1 | 0 |
| HCFC–141b (pptv) | 12 | 16 | 0 |
| Halon–1301 (pptv) | 1.4 | 3.0 | 0.9 |
| Halon–1211 (pptv) | 1.1 | 3.0 | 0.2 |
| $CH_3Cl$ (pptv) | 600 | 550 | 600 |
| $CH_3Br$ (pptv) | 10 | 7.34 | 10 |
| $CH_4$ (ppbv) | 2052 | 1997 | 2793 |
| $N_2O$ (ppbv) | 333 | 335 | 371 |
| $CO_2$ (ppmv) | 405 | 417 | 509 |

## 2.2 Model Description

The UIUC 2–D chemical-radiative-transport model is a zonally-averaged model of the chemistry and physics of the global atmosphere. The model is often used to study human related and natural forcings on the troposphere and stratosphere, but, because it is zonally-averaged, the analysis of tropospheric processes is limited. The model determines the atmospheric distributions of 78 chemically active atmospheric trace constituents. The model domain extends from pole to pole and from the ground to 84 km. A grid element in the model represents 5° of latitude and 1.5 km in log-pressure altitude. In addition to 56 photolytic reactions, the model incorporates 161 thermal reactions in the chemical mechanism; including heterogeneous reactions (e.g., see Wuebbles et al., 2001, or Wei et al., 2001). Reaction rates and photolysis cross-sections in the model are based on recommendations from NASA's Chemical Kinetics Review Panel (e.g., DeMore et al., 1997; Sander et al., 2000).

The transport of chemical species is accomplished through advection, turbulent eddy transport, and convection. Transport of species in the model is self-consistently calculated using the predicted model ozone (and other radiatively important species) and seasonally varying climatological temperatures (based on NCEP analyses). Model transport fields are evaluated by combining the zonal mean momentum equation and the thermodynamic equation into a form that, along with the thermal wind equation yields a second order Poisson diagnostic equation for the residual mean meridional stream function. The right hand side of the stream function equation includes the net heating rate term and all wave forcings. The net heating rate is calculated knowing the temperature and chemical species distributions and includes latent heating. Planetary waves for wave numbers 1 and 2 are included. Stratospheric values of $K_{yy}$ are calculated using the planetary wave dissipation rate and vorticity for both wave numbers 1 and 2. Values of $K_{zz}$ due to gravity waves are evaluated. Larger diffusion coefficients are assigned to the troposphere to mimic fast tropospheric mixing. The model uses a seasonally varying tropospheric $K_{yy}$. Convective transport in the model is based on the climatology of Langner et al. (1990).

The latest version of the UIUC 2–D model, labeled the 2002 version, has some key improvements incorporated in it. All of the upgraded components of this version are briefly described in table 2. Major upgrades to the solution technique of residual mean meridional circulation (RMMC) and the treatments of atmospheric dynamics were made through better representation of the effects of planetary waves and a more accurate method for determining the RMMC. The treatment of planetary waves with wave numbers 1 and 2 have been updated with better data-based boundary topography and boundary winds. Latent heating and the sensible heat flux are specified based on more physically meaningful analyses. An accurate and fast long wave radiation code for the height of surface to 60 km is adopted in the radiation part of the model. The improvements in the treatment of the infrared radiation and RMMC solution technique are discussed in Choi and Youn (2001). The zonally averaged temperature and wind fields are specified based on 6 year climatology of the United Kingdom Meteorological Office (UKMO) reanalysis data. In addition, background diffusion coefficients, which cannot be explicitly obtained in the model, are also tuned for the "leaky pipe" model and the model barrier between tropics, mid-latitudes, and polar regions.

In the current version of the model the chemistry has been updated according to the NASA recommendations (Sander et al., 2000). This particularly affects the nitrogen oxide chemistry, the $N_2O_5$ and $ClONO_2$ hydrolysis and several HOCl and HCl reactions. HOBr and HOCl cross-sections and the $O_3$ photolysis quantum yields are updated as well.

All of these changes in the model have resulted in the improved representation of the distributions of age of air, which means better model transport in the "age of air" concept (Hall and Plumb, 1994; Hall et al., 1999). Figure 1 represents simulations of mean age by the improved models of 2001 version to 2002 version. The upgraded components make the model mean age distribution closer to the observed features described in "Models and Measurements II" (Park et al., 1999). Figure 1(d) is the mean age distribution of the 2002 version of UIUC 2–D model. It shows the tropical pipe structure in the tropics. The older mean age in the higher latitudes and altitudes than those in M & M II is seen and thought to be closer to the observed age of air. For example around 23 to 25 km the mean age of the current model in the Polar Regions is larger than the previous versions, which shows the improved performance of the current model in the vicinity.

***2.2.1 Comparison of the new UIUC 2–D Model Results with Measurement Data***.—The distribution of the chemical species determined from the 2002 version of the model have been compared with available observations, such as the HALOE climatological data obtained by six years average of 1993 to 1998 of satellite measurements. The broad patterns and magnitudes of model $CH_4$, $H_2O$, HCl, and $O_3$ distributions agree well with HALOE observations (fig. 2). The agreement in the equatorial region looks outstanding, especially in the upper stratosphere. In the mid-latitudinal lower and middle stratosphere the model trace gases show a smaller horizontal gradient than the HALOE data due to uncertain planetary wave diffusion in the model. Model trace gases in the equatorial lower stratosphere show some bulge and isolation from mid-latitude, although the degree of the bulge is smaller.

For $NO_x$, when the model output data is compared with the HALOE data, as shown in figure 3, we see that the model compares extremely well with the observations up to 30 km altitude, thus conforming well to the satellite observations in the lower stratosphere, the region of interest for the aircraft studies. There are, however, large disagreements in the middle and upper stratosphere region, suggesting that the current model has an error in representing $NO_x$ chemistry in this region. We are currently investigating the cause for the discrepancy. Since most of the aircraft emissions will be in upper troposphere lower stratosphere region, it is reasonable to say that the current version of the UIUC 2–D model captures $NO_x$ sufficiently well in the region of concern to be a very useful tool for the purpose of aircraft studies.

TABLE 2.—A BRIEF DESCRIPTION OF THE IMPROVED METEOROLOGICAL COMPONENTS IN THE UIUC 2–D MODEL

| Upgraded Model Components | Description | References |
|---|---|---|
| RMMC ($\bar{v}^*$, $\bar{w}^*$) | Two schemes of residual mean meridional circulation (RMMC), which target accurate residual circulation in the whole model domain, are applied adequately according to the height levels. It uses both thermodynamic energy equation and continuity equation among four TEM equations avoiding tricky and uncertain wave forcings. | Choi (1995) Choi and Youn (2001) |
| Longwave heating rates $Q_{IR}$ | Fast and accurate longwave radiation code for the height range of surface to 60 km is merged to the radiation part of the model. Absorption by $CO_2$, $O_3$, $H_2O$, $CH_4$, and $N_2O$ are atmospheric absorber in the infrared code. | Olaguer et al. (1992), Gettelman et al. (1997) |
| Latent & sensible heating rates $Q_{latent}$ | The results of SNU AGCM (Seoul National University AGCM) are adopted. It is more physical than those from the previous crude parameterization because the algorithm used in the AGCM contains full physical processes in sophisticated manner. | Arakawa and Schubert (1974), Matsuno (1995), Kim (1999) |
| UKMO meteorological fields | The zonally averaged monthly–mean climatologies of wind ($\overline{U}$) and temperature ($\overline{T}$) field from 6 years of UKMO reanalysis data are used in the model through Fourier time interpolation. | Swinbank and O'Neill (1994) Manney et al. (1996) |
| Planetary wave model | Rayleigh friction coefficient is found to be very sensitive to amplitudes of wave amplitude in the planetary wave model, and so tuned for the better simulation of planetary waves. Planetary wave number 2 was considered as well as wave number 1 with real boundary topographical values and boundary.<br>$K_{yy}$ by planetary wave breaking is parameterized following Garcia (1991), but from full expression of dissipation rates. | Garcia (1991) Garcia et al. (1992) Randel & Garcia (1994) Choi (1996) Li et al. (1995) Nathan et al. (2000) |
| background $K_{yy}$ | The background values of $K_{yy}$ outside planetary wave breaking region have influence on the global distribution of trace gases. Values of Background $K_{yy}$ $5\times10^3$ $m^2$ $s^{-1}$ were chosen for "tropical pipe model" in 2001 model, but these values made tracer distribution away from observed distribution. And so background $K_{yy}$ values are increased and tuned especially in the equatorial region considering height levels such as $0.13\times10^6$ $m^2$ $s^{-1}$ from tropopause to 21 km, $0.07\times10^6$ $m^2$ $s^{-1}$ from 21 to 35 km, and $0.1\times10^6$ $m^2$/s above 35 km for "leaky pipe model."<br>The various different background values of $K_{yy}$ between tropics and mid–latitudes are tested and then properly specified. Some changes in the troposphere are also done. | Schoeberl et al. (1997) Shia et al. (1998) Li & Waugh (1999) Schneider et al. (2000) Jones et al. (2001) |
| $K_{zz}$ | Vertical diffusion coefficient $K_{zz}$ values in the troposphere and lower stratosphere were changed. A lower limit of $K_{zz}$ of 0.01–0.02$m^2s^{-1}$ in the lower stratosphere following the observational analysis of Hall and Waugh (1997) and Mote et al. (1998) was specified. But it makes little difference in the model distribution of trace gases. | Hall et al. (1999) Shia et al. (1998) Bacmeister et al. (1998) Fleming et al. (1999) |

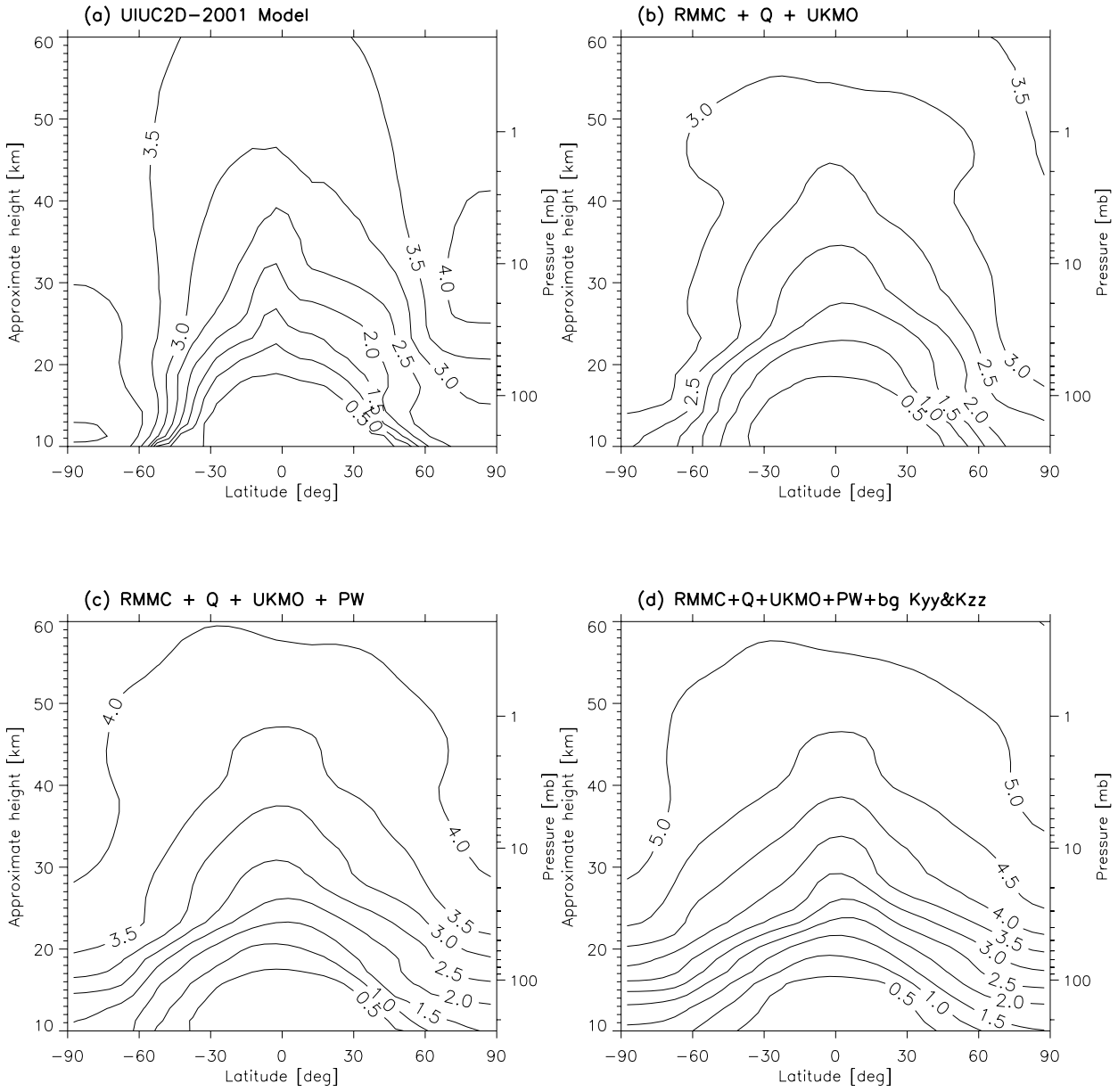


Figure 1.—Mean age distributions derived from the age spectrum simulated by improved models. (a) 2001 model and the models (b) with UKMO data and the improvement of circulation and long wave radiation, (c) with the improvement of planetary wave model, and (d) with background and tropospheric $K_{yy}$ and $K_{zz}$ tuned. Modifications from (b) to (d) are accumulatively added to the 2001 model.

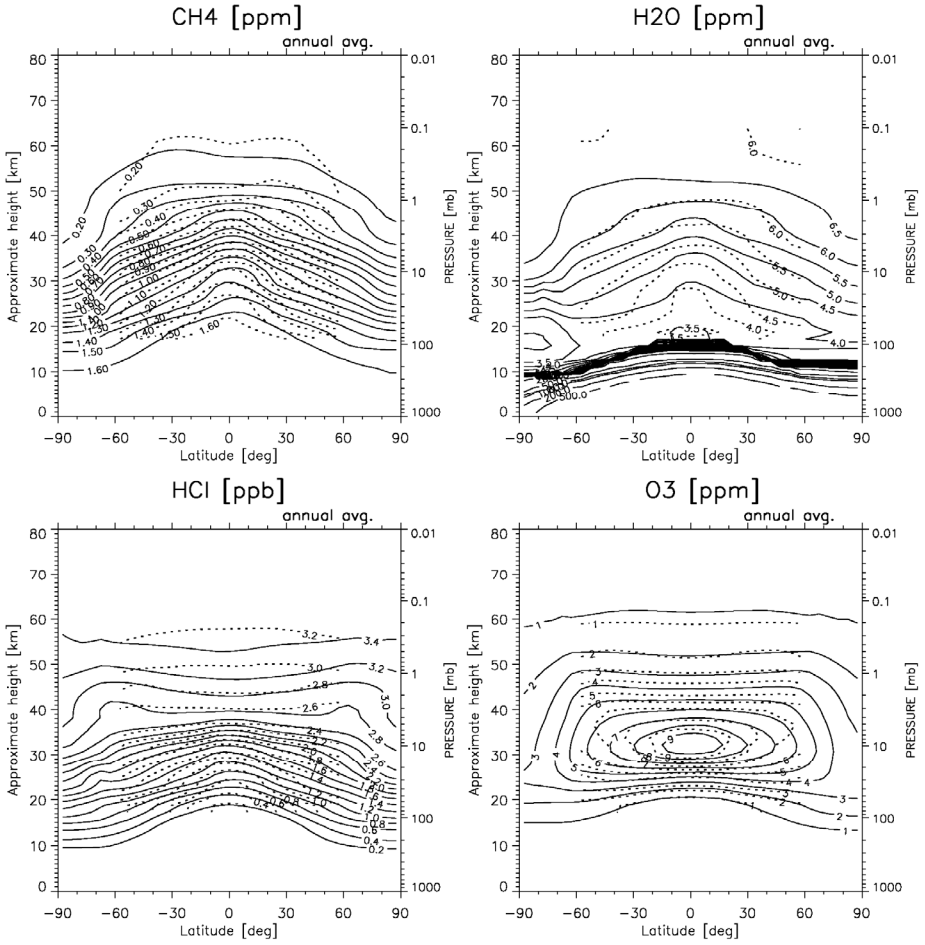


Figure 2.—Annually–averaged zonal mean mixing ratios of (a) CH4 (ppm), (b) H2O (ppm), (c) HCl (ppb), and (d) O3 (ppm) from 2002 UIUC 2–D CRT model (solid lines) and 6-year-averaged HALOE observation (dotted lines).

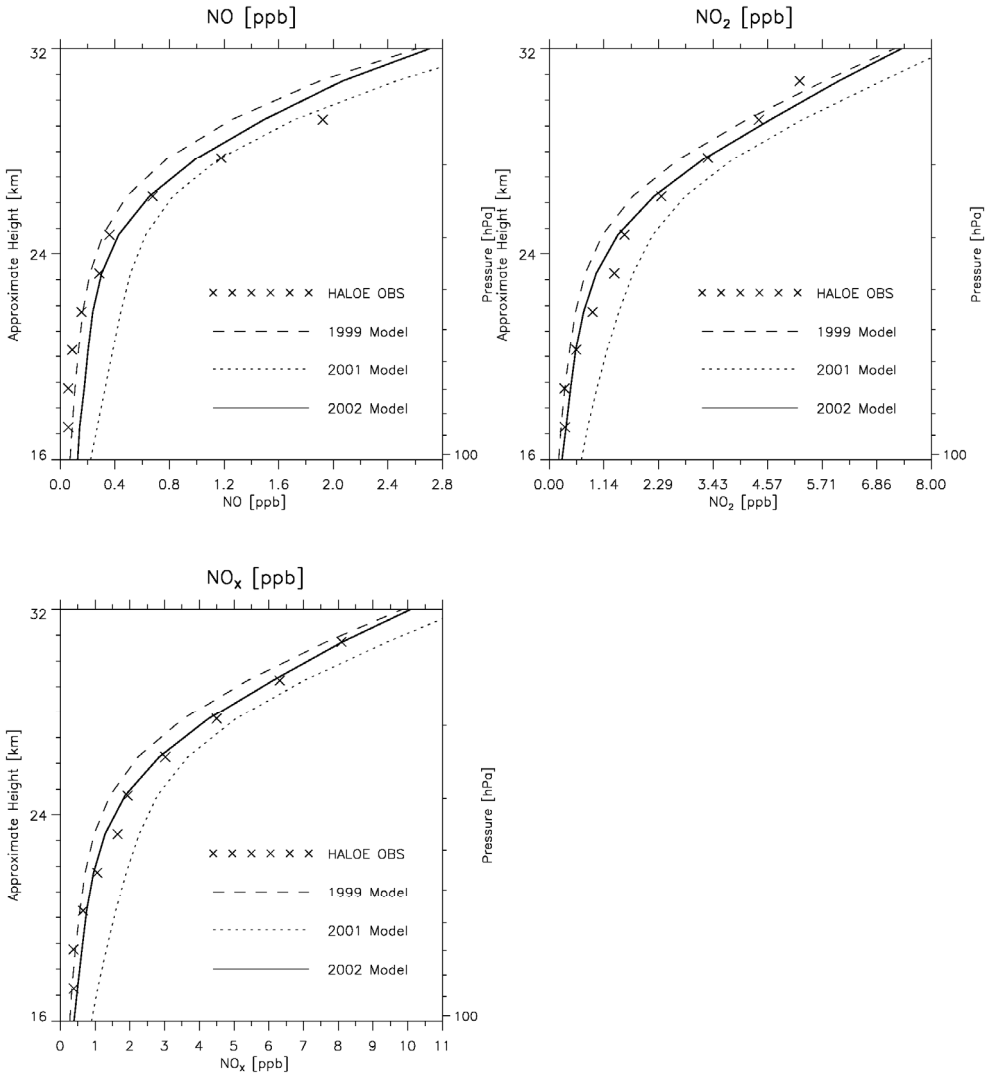


Figure 3.—Vertical profiles of annual mean values for (a) NO, (b) $NO_2$, and (c) $NO_x$ from the 1999 version (dashed), 2001 version (dotted), and 2002 version (solid) of model and 6-year-averaged HALOE observations (cross mark) in the Northern hemispheric mid-latitude (32.5 to 57.5 N).

# 3. Results and Discussion

## 3.1 Comparison of Model Results with IPCC

The current version of the UIUC 2–D model generally shows much higher sensitivity to $NO_x$ emissions from HSCT aircraft than the IPCC (1999) assessment models (using earlier scenarios compared to those used otherwise in this study). The overall difference with the 1999 analyses is largely due to several changes in the recommended chemistry for nitrogen oxides in the lower stratosphere, resulting in an increased sensitivity of $NO_x$ emissions on stratospheric ozone. The differences in the results for the Southern Hemisphere can be attributed to the enhancements in the treatment of dynamical processes in this version of the model, with resulting increased transport of $NO_x$ across the equatorial region.

All the results are obtained from steady state model simulations where the model is run for 10 years with the same species input, heating rates input and climatological input files and differing aircraft emission input files according to the scenarios.

Table 3 gives the results of the two versions of the UIUC 2–D model for Northern and Southern Hemispheres separately of total column ozone change (in percentage) along with the results of all the other 2–D model assessments as reported in IPCC (1999).

The northern hemisphere value is in good agreement with the rest of the model results for the S1b ($H_2O$ only) scenario but for most of the other scenarios (S1c, S1d, S1e, and S1i) the percentage decrease in column ozone is slightly higher that the other model results. A much higher decrease in ozone (–0.95 percent) is seen for a greater fleet size [S1i scenario (fleet size = 1000, E.I. ($NO_x$) = 5)]. But this is similar to that of GSFC 2–D (NASA Goddard Space Flight Center 2–D model) result (–0.9 percent) and close to the AER (Atmospheric and Environmental Research model) result (–0.7 percent). The highest northern hemisphere column ozone change is seen for the S1e scenario (–1.39 percent) which has an E.I. ($NO_x$) = 15 g/kg of fuel. Thus the current version of the UIUC 2–D model has a more acute ozone depleting chemistry arising from nitrogen oxides ($NO_x$). This is essentially because of the chemistry update done in this version as mentioned above in the model description section.

The Southern Hemisphere values for the percentage decrease in total column ozone are much higher for our 2–D model than most of the other assessment models except for GSFC 2–D, which has similar, or even higher ozone depletion values reported for Southern hemisphere. Actually the Southern Hemisphere response to HSCT emissions depends on the transport characteristics of the model, particularly because HSCT emissions occur far from the Southern Hemisphere vortex. Global transport characteristics determine the fraction of HSCT emissions, which eventually are transported into the Southern Hemisphere winter polar vortex. (Kinnison et al., 2001). Thus the high value obtained for the Southern Hemisphere from the current version of the UIUC 2–D model can be accounted for because of the different representation of the transport phenomenon due to the changes made in the dynamics of the model.

Figure 4 shows percentage change in ozone profile for S1c [fleet size = 500, E.I. ($NO_x$) = 5] relative to D[subsonic aircraft only] in June 2015. The broad distribution pattern matches with most of the 2–D models reported in IPCC (1999) as shown in figures 4 to 6(c) (IPCC, 1999). There is an ozone formation maximum (~0.75 percent) around the equatorial region near 20 km altitude and decrease of 0.5 to 0.75 percent near the Northern Hemisphere higher latitudes in the upper troposphere lower stratosphere region. This is expected due to the fact that most of projected air traffic would be in the Northern Hemisphere. But even if the HSCT aircraft emissions are primarily in the Northern Hemisphere mid-latitude region, the maximum ozone loss is observed at Northern Hemisphere high latitudes. This is because of the effects of atmospheric transport processes.

Figure 5 depicts the percentage change in total column ozone over a year for the S1c scenario from the UIUC 2–D model. The plot is comparable to the IPCC (1999) Figures 4 to 6(d). There is an ozone depletion peak near the southern polar region around the month of October. It is also noteworthy to see

TABLE 3.—PERCENTAGE CHANGE IN TOTAL COLUMN OZONE FOR EACH ASSESSMENT MODEL (IPCC, 1999) WHERE SIX ≡ SUBSONIC + SUPERSONIC SCENARIO (2015), D ≡ 2015 BASE, D9 ≡ 2050 BASE, SA5 ≡ 10% $SO_2$ GAS TO PARTICLE CONVERSION FOR 500 HSCT FLEET SIZE AND SA6 ≡ 10 PERCENT $SO_2$ GAS TO PARTICLE CONVERSION FOR 1000 HSCT FLEET SIZE, NH AVG ≡ NORTHERN HEMISPHERE AVERAGE, SH AVG ≡ SOUTHERN HEMISPHERE AVERAGE NR≡ NO RESULTS

| IPCC scenario | Fleet Size | E.I. ($NO_x$) (g/kg) | Ref. Atmos | | AER –2D | GSFC –2D | UNIVAQ –2D | LLNL –2D | CSIRO –2D | THINAIR –2D | UIUC 2–D –1999 | UIUC 2–D –2002 |
|---|---|---|---|---|---|---|---|---|---|---|---|---|
| | | | | | | | | | | | | |
| S1b | 500 | 0 | D | NH Avg | –0.6 | –0.4 | –0.4 | –0.3 | –0.3 | NR | –0.37 | –0.29 |
| ($H_2O$ only) | | | | SH Avg | –0.3 | –0.8 | –0.2 | –0.3 | –0.07 | NR | –0.25 | –0.20 |
| S1c | 500 | 5 | D | NH Avg | –0.3 | –0.4 | –0.002 | –0.2 | –0.2 | –0.2 | –0.34 | –0.49 |
| | | | | SH Avg | –0.1 | –0.8 | 0.02 | –0.2 | –0.1 | –0.2 | –0.10 | –0.30 |
| S1d | 500 | 10 | D | NH Avg | –0.3 | –0.6 | 0.2 | –0.3 | –0.3 | –0.5 | –0.49 | –0.70 |
| | | | | SH Avg | –0.1 | –0.7 | 0.1 | –0.1 | –0.2 | –0.3 | 0.01 | –0.29 |
| S1e | 500 | 15 | D | NH Avg | –0.3 | –0.8 | 0.4 | –0.4 | –0.5 | –0.9 | –0.76 | –1.39 |
| | | | | SH Avg | –0.05 | –0.7 | 0.2 | –0.01 | –0.3 | –0.5 | 0.09 | –0.67 |
| S1i | 1000 | 5 | D | NH Avg | –0.7 | –0.9 | –0.06 | –0.5 | –0.5 | –0.4 | –0.66 | –0.95 |
| | | | | SH Avg | –0.3 | –1.4 | 0.005 | –0.3 | –0.2 | –0.3 | –0.19 | –0.58 |
| S1k | 500 | 5, SA5 | D | NH Avg | –0.8 | –0.7 | –0.2 | –0.5 | –0.4 | NR | –0.48 | –0.51 |
| | | | | SH Avg | –0.3 | –0.9 | –0.05 | –0.3 | –0.1 | NR | –0.22 | –0.37 |
| S9h | 1000 | 5,SA6 | D9 | NH Avg | –0.8 | –1.1 | –0.3 | –0.6 | –0.6 | NR | –0.73 | –0.81 |
| | | | | SH Avg | –0.3 | –1.5 | –0.09 | –0.4 | –0.4 | NR | –0.24 | –0.59 |

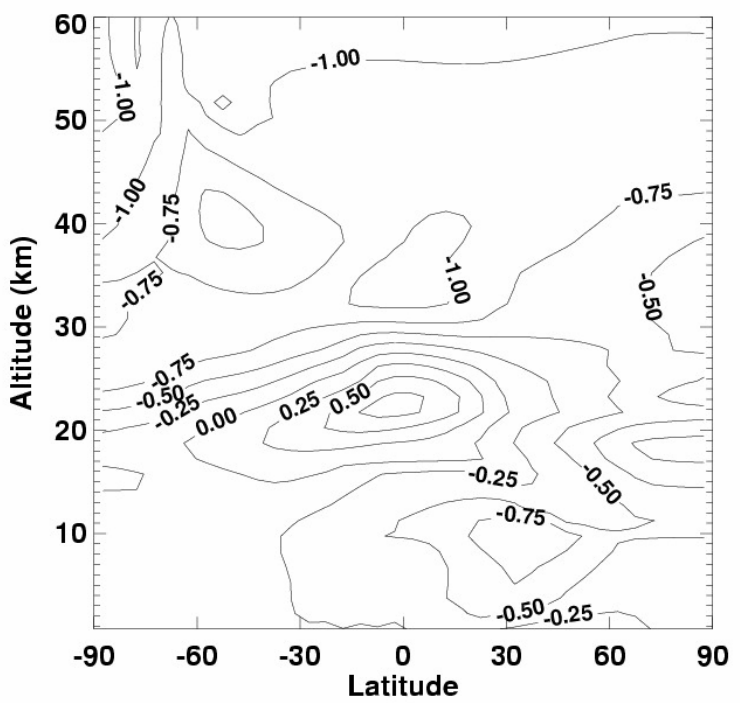


Figure 4.—Percentage change in ozone profile for S1c [E.I. ($NO_x$) = 5, 500 supersonic + subsonic aircraft] relative to D[subsonic aircraft only] in June 2015 from the current version of the UIUC 2–D model.

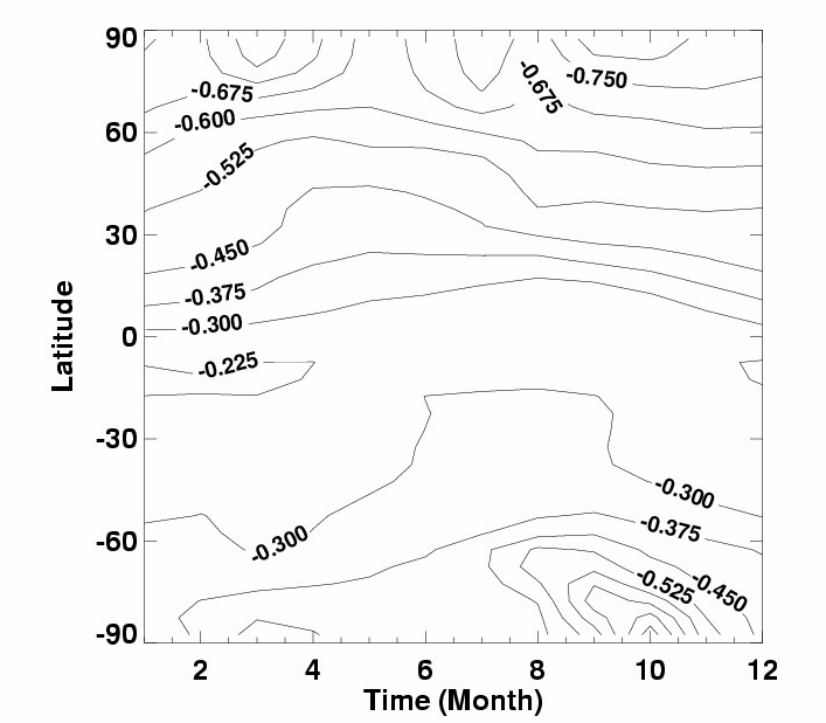


Figure 5.—Percentage total column ozone change for S1c [E.I. ($NO_x$) = 5, 500 supersonic + subsonic aircraft] relative to D [subsonic aircraft only] from the current version of the UIUC 2–D model.

two depletion maxima near the northern hemisphere contrary to the single maxima of ozone depletion predicted by the other models used in the IPCC (1999).

The change in water vapor concentration (in ppmv) for the S1c scenario is shown in figure 6. The water vapor change pattern shows very close similarity with the IPCC (1999) figures 4 to 6(b). A maximum concentration of ~ 0.6 ppmv is predicted by our model around 30 to 60 °N latitudes which matches with most of the 2–D models results in IPCC, 1999 report. The water vapor distribution shown in figure 6 is only above the tropopause.

The column ozone sensitivity to supersonic emission of $NO_x$ can be seen in figure 7. It compares between the two versions of the UIUC 2–D model and all the 2–D assessment models (IPCC, 1999). The 2002 version of the UIUC 2–D model predicts more depletion of ozone due to addition of $NO_x$ than the 1999 version as well as the other models reported in 1999 IPCC report, especially for E.I. ($NO_x$) = 10 and 15 g/kg of fuel. This conforms to the chemistry upgrades done in the current version of the UIUC 2–D model. Thus the UIUC 2–D model shows quite a large sensitivity to addition of $NO_x$ in the range after E.I. ($NO_x$) = 5 to 15g/Kg of fuel. In general the model derived $O_3$ change is in better agreement among participating models at E.I. ($NO_x$) = 5 and 10 g/kg of fuel. The spread is considerable at E.I. ($NO_x$) = 15 g/kg of fuel amongst the models.

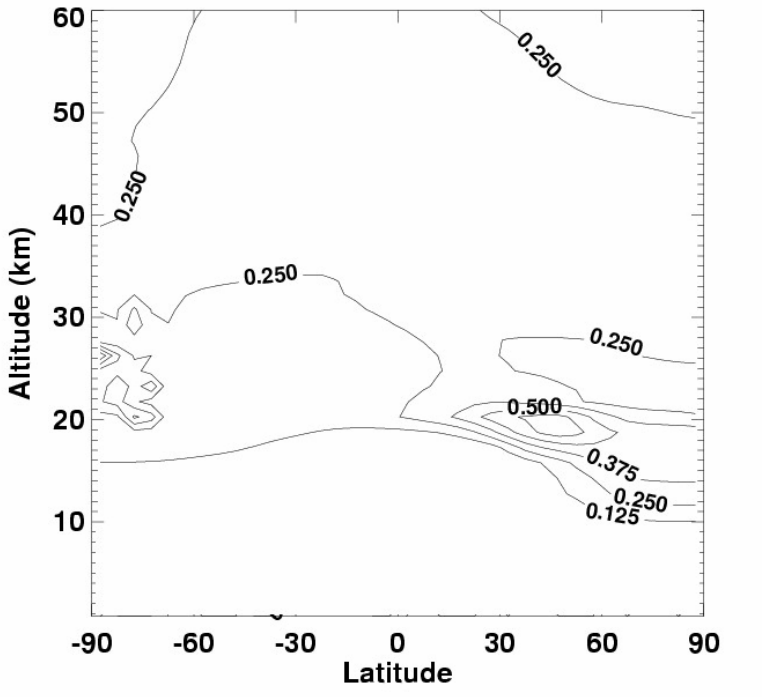


Figure 6.—$H_2O$ change (ppmv) for S1c [E.I. ($NO_x$) = 5, 500 supersonic + subsonic aircraft] relative to D[subsonic only] in June 2015 from the current version of the UIUC 2–D model.

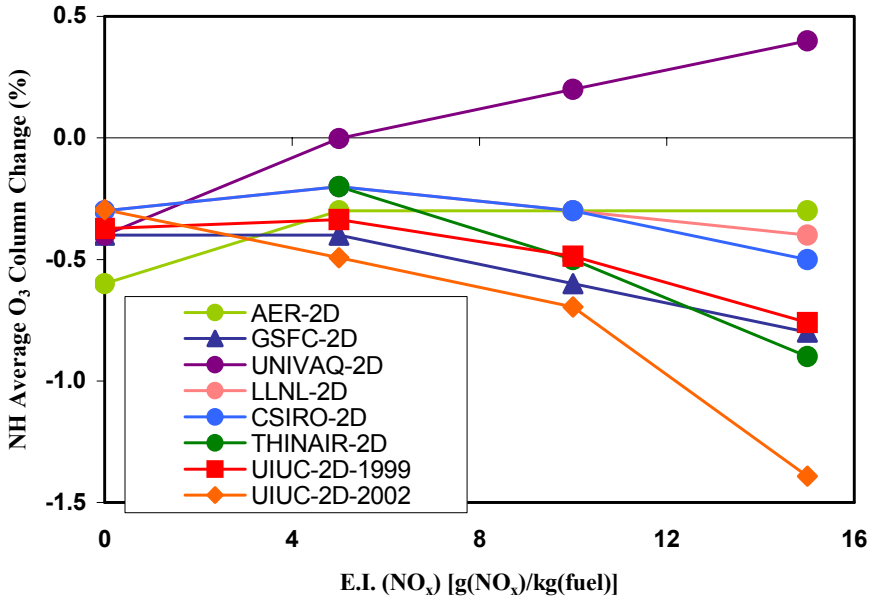


Figure 7.—Northern Hemisphere total $O_3$ column change as a function of E.I. ($NO_x$) in 2015 for an HSCT fleet size of 500 aircraft for all the IPCC (1999) model results and the three versions of the UIUC 2–D model.

### 3.2 HSCT Type Scenario Results

A total of 24 scenarios have been evaluated for the latest HSCT type fleet scenarios from Baughcum et al. (2002). All the results are obtained from steady state model simulations where the model is run for 10 years the same way as the previous scenarios have been studied. Table 4 gives the total column ozone change, global and for the two hemispheres separately, for two cases of fuel burns each evaluating four different cruise altitudes and three different E.I. ($NO_x$) cases.

In table 4, for the two different fuel burns and E.I. ($NO_x$) cases, there is no net total ozone depletion for the cruise altitude band 13 to 15 km. This can be attributed to the fact that in the upper troposphere and lowest altitudes of the stratosphere, ozone can be formed instead of destroyed by higher nitrogen oxide concentrations due to chemistry similar to the smog cycle. Thus, for any given latitude, there is a crossover point above which $NO_x$ destroys ozone and below which $NO_x$ produces ozone.

For the most likely cases for a realistic HSCT fleet, with E.I. ($NO_x$) of about 10 gm $NO_x$ per kg fuel and cruise altitudes above about 15 km, the Northern Hemisphere decrease in total ozone is less than or equal to 0.064 percent.

Table 4 shows that the impact in the Northern Hemisphere total column ozone change is much larger than the impact in the Southern Hemisphere. There is much more HSCT air traffic expected in the Northern Hemisphere compared to the Southern Hemisphere. The effect on the Southern Hemisphere ozone is larger than would be expected based on the relative amount of emissions due to transport of emissions across the equatorial region.

The maximum change in local ozone depletion amongst all the scenarios is 2.22 percent, which is found for the higher total fuel burn of 146 Mlbs/day and E.I. ($NO_x$) = 20 g/kg and the highest cruise altitude band of 19 to 21 km. For the lower E.I. ($NO_x$) cases of 5 and 10 g/kg of fuel with the same fuel burn and same cruise altitudes, the maximum local ozone depletion are 0.49 and 1.01 percent, respectively.

Figure 8 depicts the total column ozone change for a fleet of HSCT type aircraft flying at a cruise altitude of 19 to 21 km for a total fuel burn of 146 Mlbs/day and E.I. ($NO_x$) = 20 g/kg of fuel relative to

TABLE 4.—PERCENTAGE CHANGE IN OZONE FOR HSCT TYPE SCENARIOS RELATIVE TO 2020 BACKGROUND ATMOSPHERE. NH AND SH CORRESPOND TO THE TOTAL OZONE CHANGE IN THE NORTHERN AND SOUTHERN HEMISPHERES, RESPECTIVELY. GLOBAL CORRESPONDS TO THE GLOBALLY-AVERAGED CHANGE IN TOTAL OZONE. MAX AND MIN CORRESPOND TO THE MAXIMUM (MOST POSITIVE) AND MINIMUM (MOST NEGATIVE) CHANGE IN LOCAL OZONE THROUGHOUT THE STRATOSPHERE.

| Fuel burn | E.I. ($NO_x$) | | Altitude bands (km) | | | |
|---|---|---|---|---|---|---|
| Mlbs/day | g/kg of fuel | | 13 to 15 | 15 to 17 | 17 to 19 | 19 to 21 |
| | | | | | | |
| 73 | 5 | NH | 0.004 | –0.015 | –0.060 | –0.110 |
| | | Global | 0.003 | –0.012 | –0.049 | –0.086 |
| | | SH | 0.002 | –0.008 | –0.038 | –0.063 |
| | | Min | 0.000 | –0.044 | –0.154 | –0.245 |
| | | Max | 0.008 | –0.001 | –0.028 | –0.047 |
| | | | | | | |
| | 10 | NH | 0.007 | –0.029 | –0.110 | –0.203 |
| | | Global | 0.006 | –0.021 | –0.086 | –0.154 |
| | | SH | 0.005 | –0.014 | –0.062 | –0.104 |
| | | Min | 0.000 | –0.083 | –0.263 | –0.508 |
| | | Max | 0.017 | 0.013 | –0.042 | –0.075 |
| | | | | | | |
| | 20 | NH | 0.014 | –0.061 | –0.222 | –0.408 |
| | | Global | 0.011 | –0.044 | –0.168 | –0.300 |
| | | SH | 0.009 | –0.027 | –0.114 | –0.192 |
| | | Min | –0.001 | –0.173 | –0.562 | –1.075 |
| | | Max | 0.032 | 0.049 | –0.035 | –0.132 |
| | | | | | | |
| 146 | 5 | NH | 0.007 | –0.032 | –0.120 | –0.216 |
| | | Global | 0.006 | –0.024 | –0.104 | –0.174 |
| | | SH | 0.005 | –0.017 | –0.088 | –0.132 |
| | | Min | 0.000 | –0.092 | –0.332 | –0.492 |
| | | Max | 0.015 | –0.001 | –0.062 | –0.096 |
| | | | | | | |
| | 10 | NH | 0.013 | –0.064 | –0.228 | –0.413 |
| | | Global | 0.011 | –0.047 | –0.183 | –0.314 |
| | | SH | 0.009 | –0.030 | –0.137 | –0.216 |
| | | Min | –0.002 | –0.179 | –0.540 | –1.005 |
| | | Max | 0.030 | 0.028 | –0.091 | –0.157 |
| | | | | | | |
| | 20 | NH | 0.023 | –0.135 | –0.487 | –0.864 |
| | | Global | 0.020 | –0.098 | –0.369 | –0.630 |
| | | SH | 0.018 | –0.060 | –0.251 | –0.397 |
| | | Min | –0.008 | –0.384 | –1.210 | –2.224 |
| | | Max | 0.049 | 0.101 | –0.052 | –0.231 |

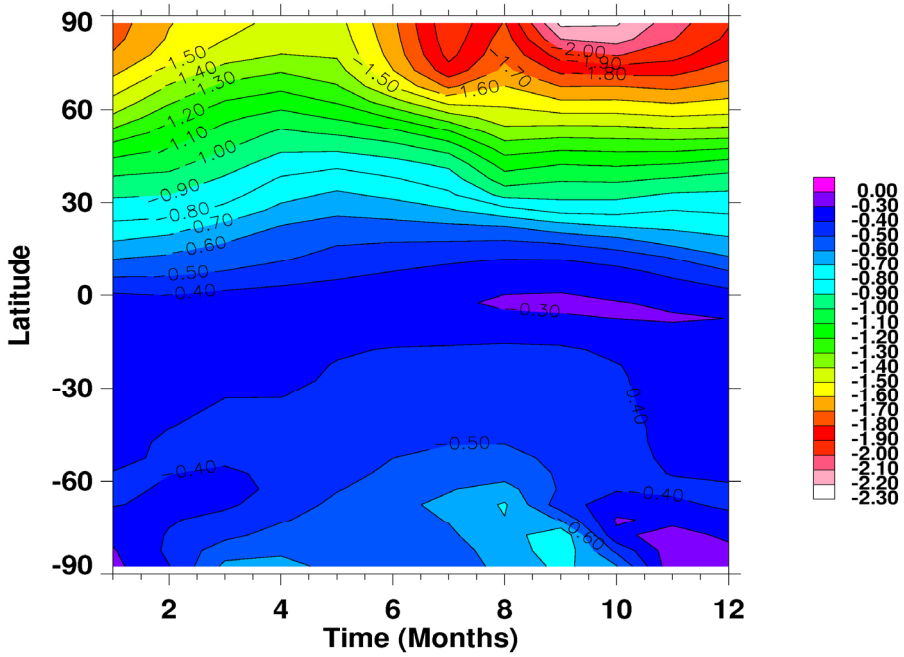


Figure 8.—Total column ozone change for a fleet of HSCT type aircraft flying at a cruise altitude of 19 to 21 km, for a fuel 146 Mlbs/day and E.I. ($NO_x$) = 20 g/kg of fuel.

the 2020 background atmosphere. The largest decrease in total ozone occurs at high Northern latitudes in the Northern Hemisphere summer and autumn months. Figure 9 is similar to figure 8 but is the case for a total fuel burn of 73 Mlbs/day. Figure 9 shows the same trend in ozone depletion but is smaller in magnitude. The ozone minimum for the 73 Mlbs/day shows values of slightly more than 0.90 percent around the North Pole region in the month of October where as for the 146 Mlbs/day case we see an ozone minimum of more than 2.0 percent around that same region.

Figures 8 and 9 represents the higher extreme of the scenarios for the two fuel burn cases. But a more likely case for a realistic HSCT fleet, with E.I. ($NO_x$) of about 10 gm $NO_x$ per kg fuel and cruise altitudes above about 15 km is depicted in figures 10 to 13.

Figure 10 represents the total column ozone change for a fleet of HSCT type aircraft flying at a cruise altitude of 17 to 19 km for a fuel burn of 146 Mlbs/day and E.I. ($NO_x$) = 10 g/kg of fuel relative to the 2020 background atmosphere. Figure 11 is for a similar scenario but for fuel burn of 73 Mlbs/day. Figures 12 and 13 shows the same for the more realistic cruise altitude of 15 to 17 km and for the two fuel burns, respectively. We see that there are two maxima of ozone depletion near the North Pole, one around July and the next around October for all these figures. For the 15 to 17 km altitude there is an ozone loss maximum of ~ 0.17 percent around the North Pole in October and little over 0.1 percent loss around the 60° N latitude region for the 146 Mlbs/day case. For the 73 Mlbs/day case the pattern looks the same but the magnitude of ozone depletion is much less.

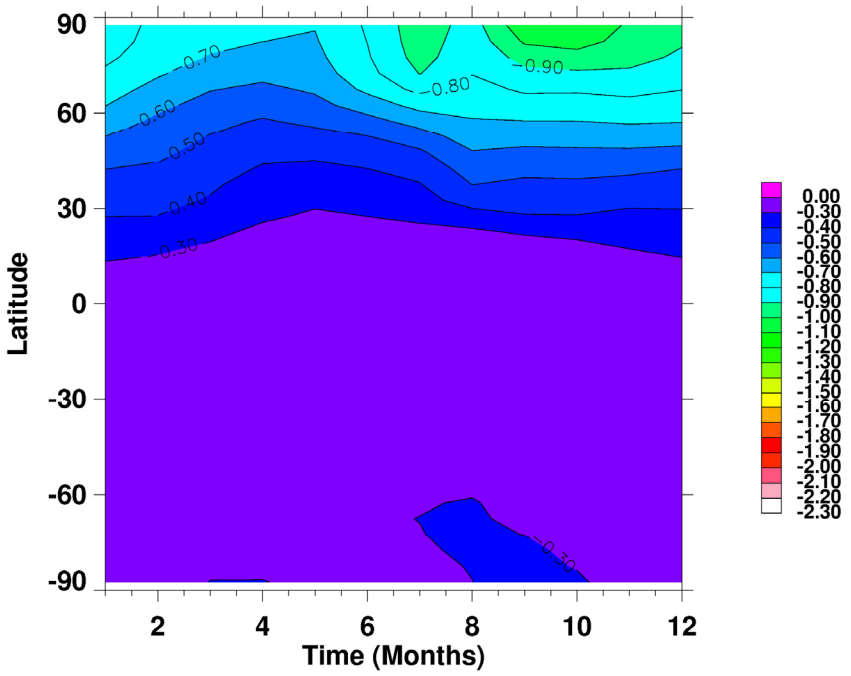


Figure 9.—Total column ozone change for a fleet of HSCT type aircraft flying at a cruise altitude of 19 to 21 km, for a fuel 73 Mlbs/day and E.I. ($NO_x$) = 20 g/kg of fuel.

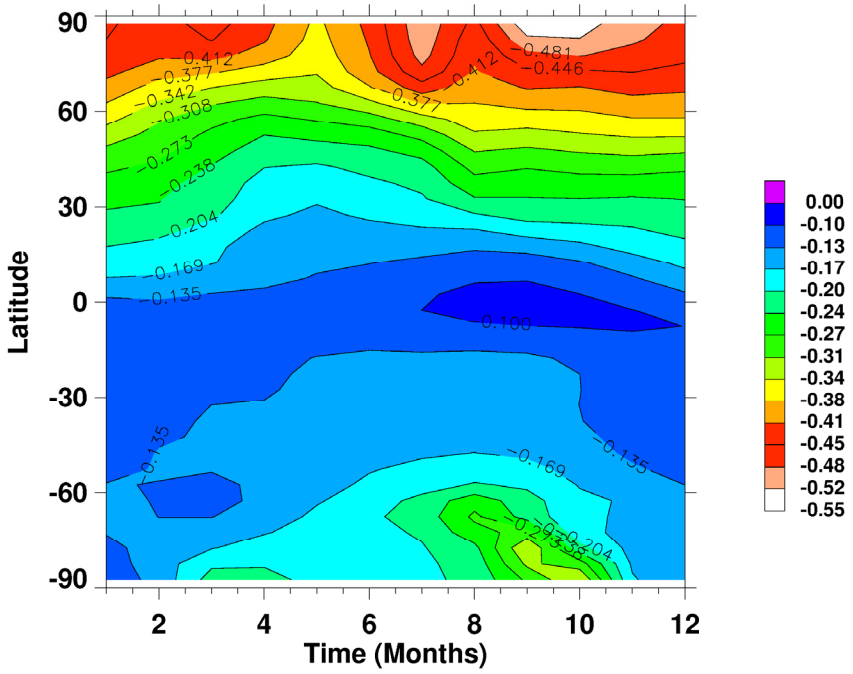


Figure 10.—Total column ozone change for a fleet of HSCT-type aircraft flying at a cruise altitude of 17 to 19 km, for a fuel burn of 146 Mlbs/day and E.I. ($NO_x$) = 10 g/kg of fuel relative to the 2020 background atmosphere.

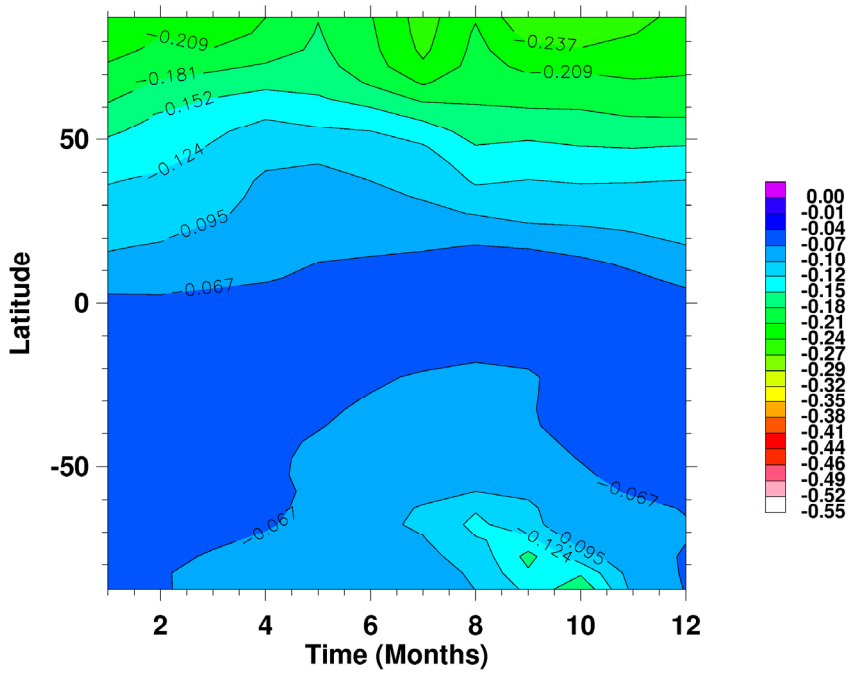


Figure 11.—Total column ozone change for a fleet of HSCT-type aircraft flying at a cruise altitude of 17 to 19 km, for a fuel burn of 73 Mlbs/day and E.I. ($NO_x$) = 10 g/kg of fuel relative to the 2020 background atmosphere.

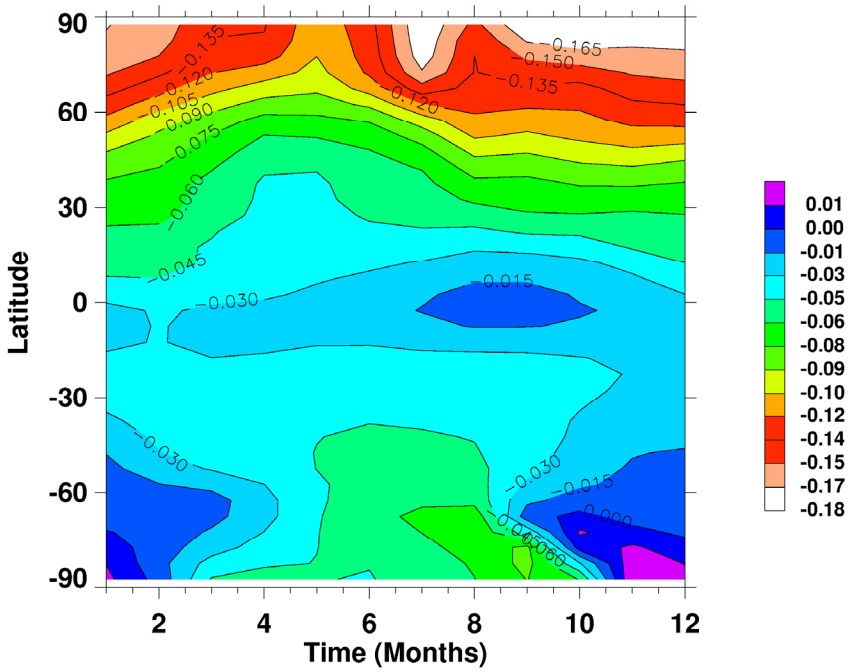


Figure 12.—Total column ozone change for a fleet of HSCT type aircraft flying at a cruise altitude of 15 to 17 km, for a fuel 146 Mlbs/day and E.I. ($NO_x$) = 10 g/kg of fuel.

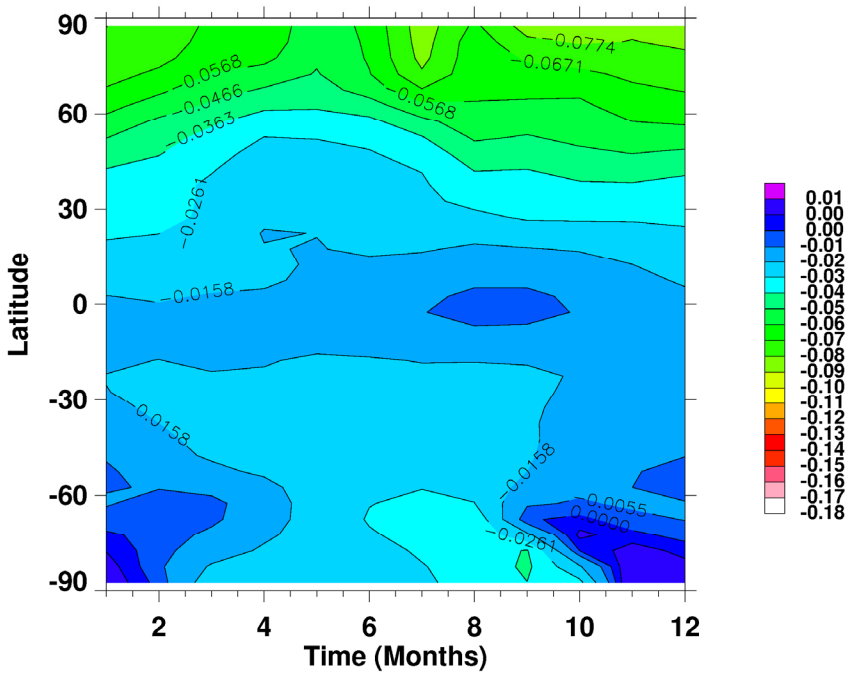


Figure 13.—Total column ozone change for a fleet of HSCT type aircraft flying at a cruise altitude of 15 to 17 km, for a fuel 73 Mlbs/day and E.I. ($NO_x$) = 10 g/kg of fuel.

Figure 14 shows the change in ozone as a function of altitude and latitude during June relative to the 2020 background atmosphere for the scenario with a cruise altitude of 19 to 21 km, a total fuel 73 Mlbs/day and E.I. ($NO_x$) = 20 g/kg of fuel. Figure 14 corroborates the fact that there is an intense ozone loss region around the Northern Hemisphere higher latitudes and around the altitude band of the aircraft emission injection. This is expected as a result of the projected aircraft emissions being primarily at mid-latitude in the Northern Hemisphere. The maximum ozone loss is observed at high latitudes of the Northern Hemisphere because of the effects of transport processes.

Figure 15 gives the change in ozone with altitude and latitude for a case similar to that in figure 14, but for a fuel burn of 73 Mlbs/day. As expected the change in ozone is smaller in figure 15 compared to the higher fuel burn scenario shown in figure 14. Figures 16 and 17 depict the same but for the more probable scenario of a fleet of HSCT type aircraft flying at a cruise altitude of 15 to 17 km for a fuel burn of 146 Mlbs/day and E.I. ($NO_x$) = 10 g/kg of fuel. In all the figures 14 to 17, a region of ozone formation from the aircraft emissions is found in the equatorial region. This increase results from increased radiation reaching lower stratospheric altitudes in the tropics due to ozone destruction at higher altitudes.

Figure 18 shows the relationship between the percentage change of total column ozone in the Northern Hemisphere relative to E.I. ($NO_x$) for the four different altitude bands and a total fuel burn of 73 Mlbs/day, while figure 19 is for a total fuel burn of 146 Mlbs/day. From these two plots it is evident that the percentage change in total column ozone holds a linear relationship with E.I. ($NO_x$) for all the four altitude bands studied. The 13 to 15 km altitude band series has a slight positive slope owing to the net formation of ozone in that region of the atmosphere.

Figures 20 to 23 depict the correlation between percentage change in Northern Hemisphere total column ozone and E.I. ($NO_x$) for the two cases of fuel burns studied (blue = 73 Mlbs/day, red = 146 Mlbs/day) for the four altitude bands starting from 13 to 21 km, respectively. From these figures, the relationship between the total column ozone change in percentage and E.I. ($NO_x$) is proven to be linear too, for the range of E.I. ($NO_x$) examined.

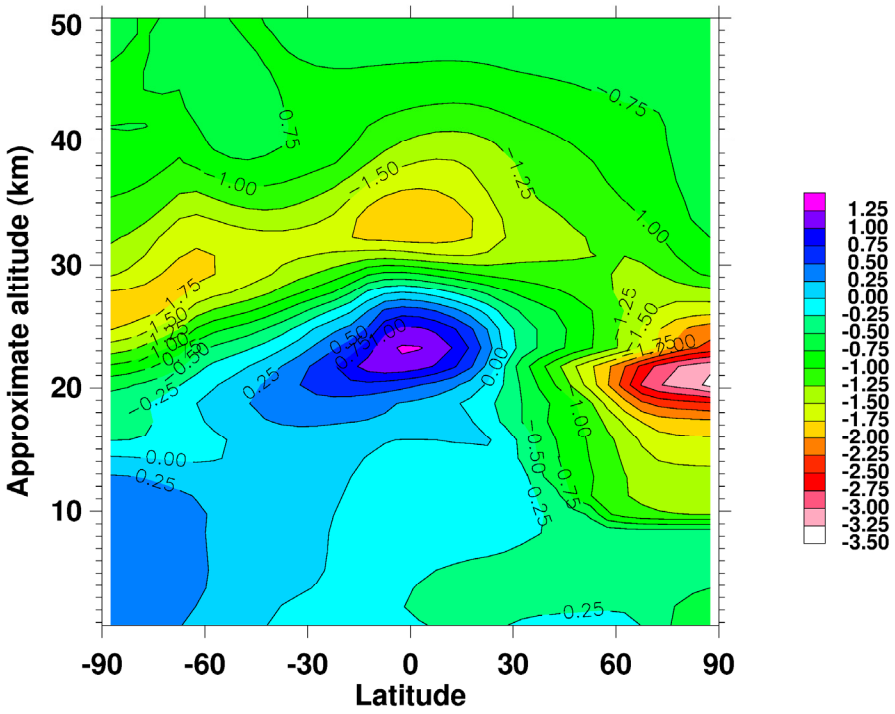


Figure 14.—Change in ozone as a function of altitude and latitude during June for a fleet of HSCT type aircraft with a cruise altitude of 19 to 21 km, a total fuel 146 Mlbs/day and E.I. ($NO_x$) = 20 g/kg of fuel.

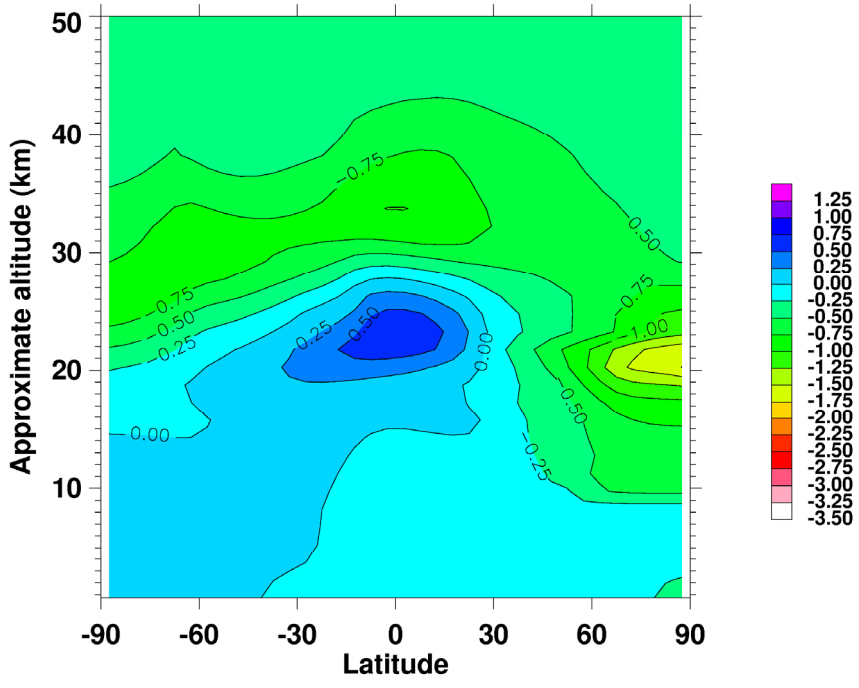


Figure 15.—Change in ozone as a function of altitude and latitude during June for a fleet of HSCT type aircraft flying at a cruise altitude of 19 to 21 km for a fuel 73 Mlbs/day and E.I. ($NO_x$) = 20 g/kg of fuel.

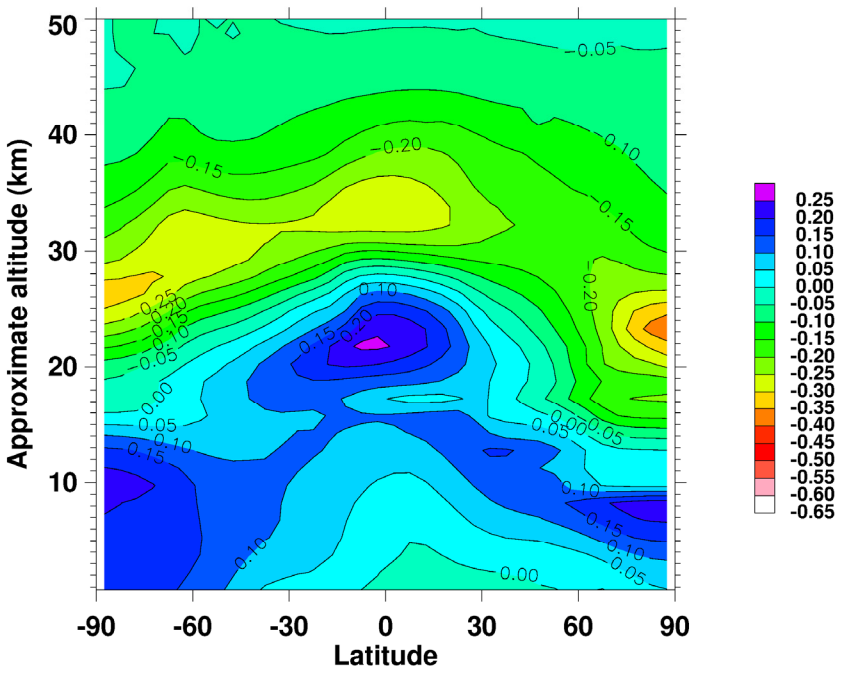


Figure 16.—Change in ozone as a function of altitude and latitude during June for a fleet of HSCT type aircraft with a cruise altitude of 15 to 17 km, a total fuel 146 Mlbs/day and E.I. ($NO_x$) = 10 g/kg of fuel.

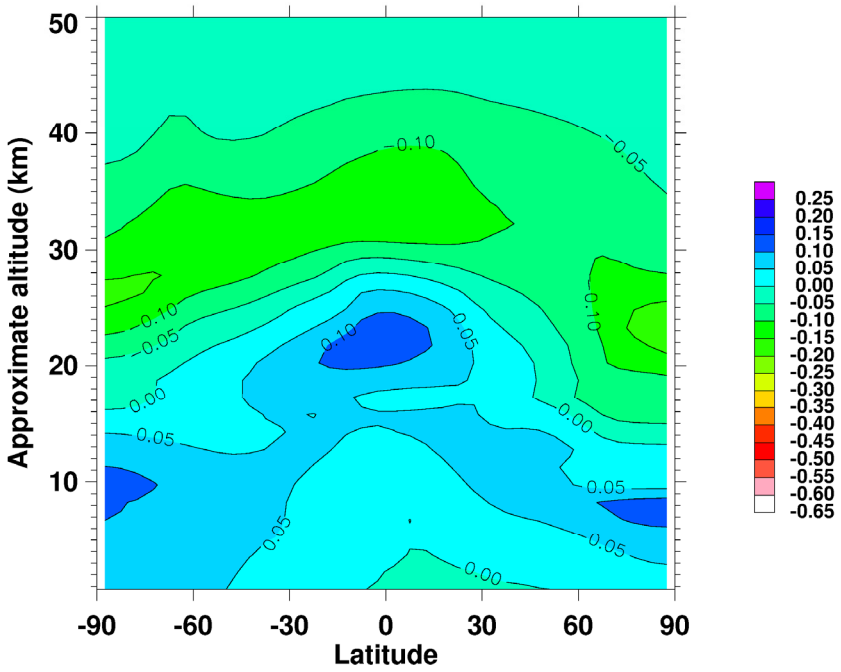


Figure 17.—Change in ozone as a function of altitude and latitude during June for a fleet of HSCT type aircraft with a cruise altitude of 15 to 17 km, a total fuel 146 Mlbs/day and E.I. ($NO_x$) = 10 g/kg of fuel.

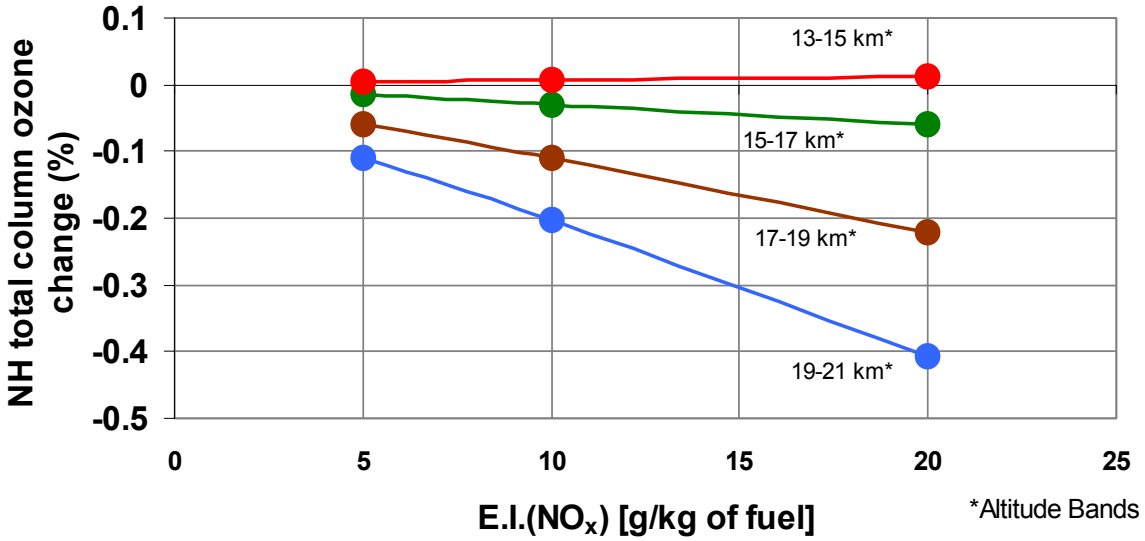


Figure 18.—Percentage change in NH total column ozone as a function of E.I. ($NO_x$) at different altitude bands for a total fuel burn of 73 Mlbs/day.

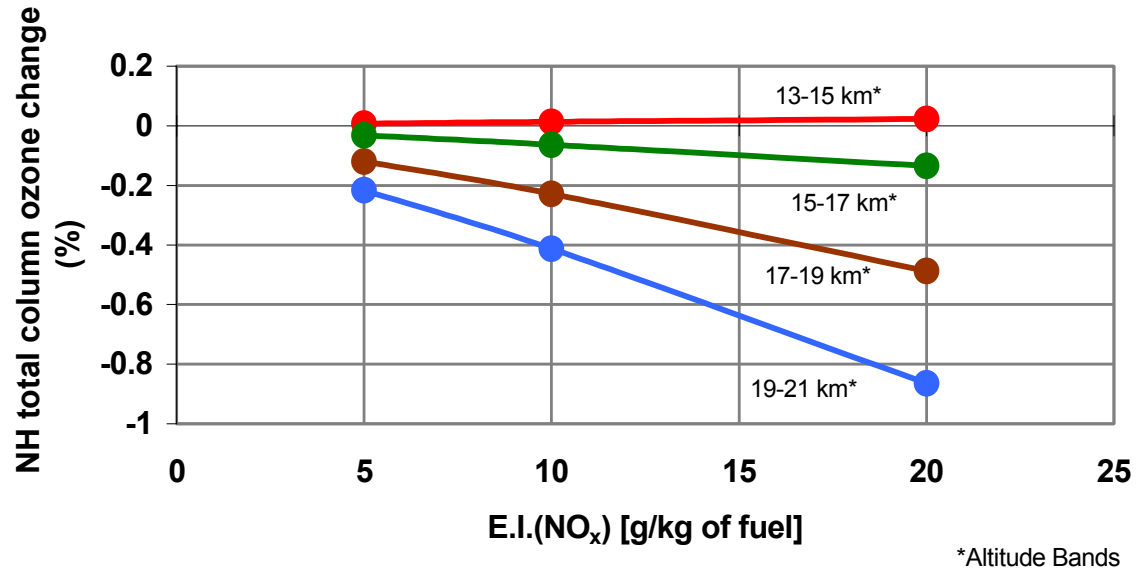


Figure 19.—Percentage change in NH total column zone as a function of E.I. ($NO_x$) at different altitude bands for a total fuel burn of 146 Mlbs/day.

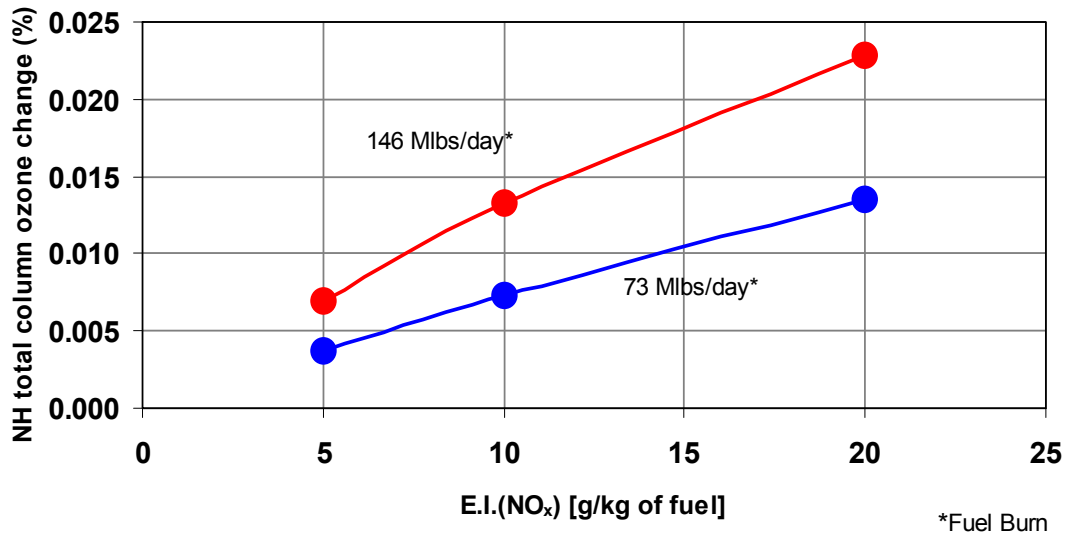


Figure 20.—Percentage change in NH total column zone as a function of E.I. ($NO_x$), for two different fuel burns for the cruise altitude band of 13 to 15 km.

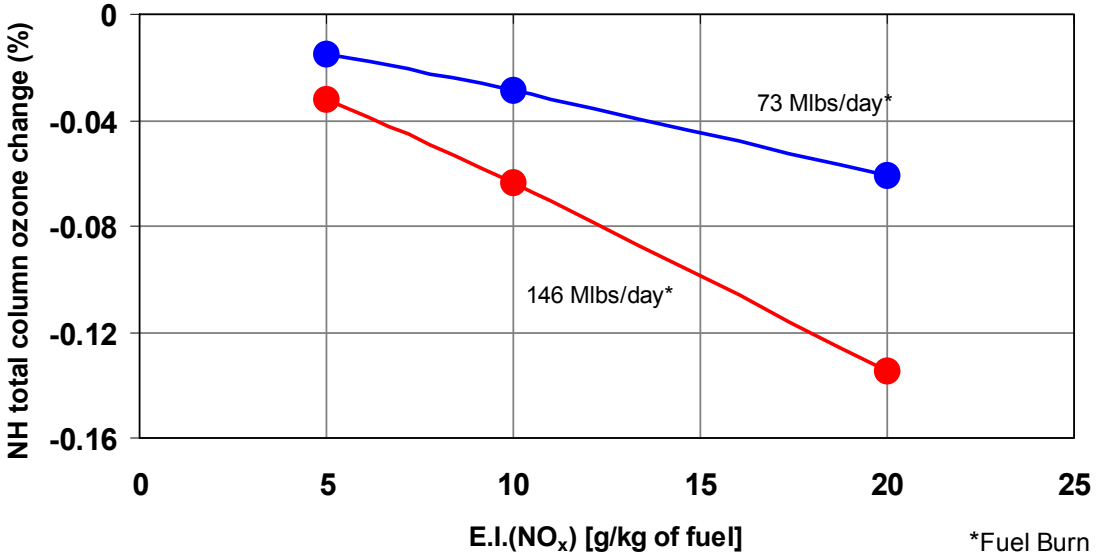


Figure 21.—Percentage change in NH total column zone as a function of E.I. ($NO_x$), for two different fuel burns for the cruise altitude band of 15 to 17 km.

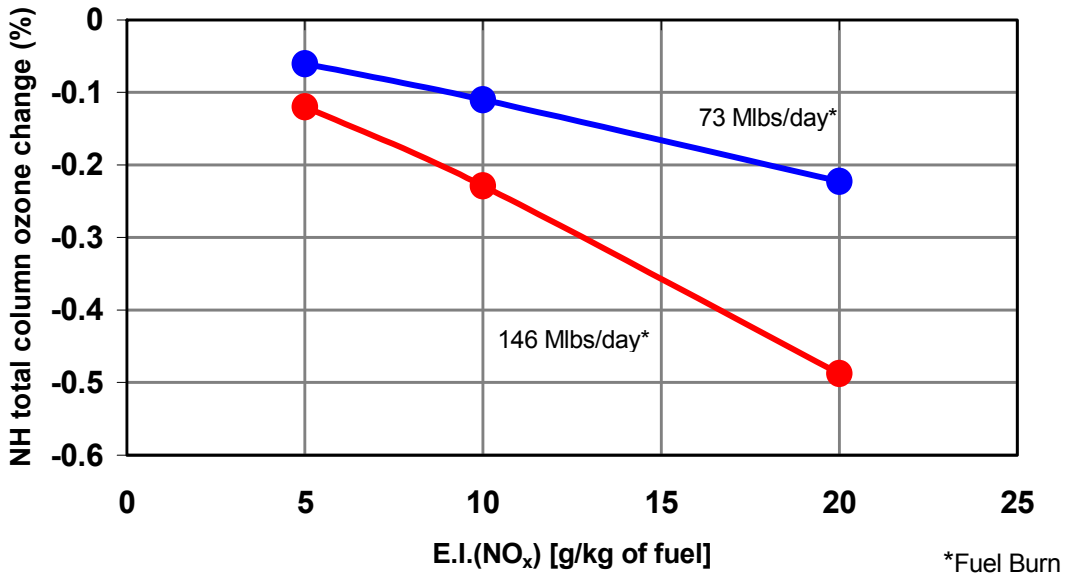


Figure 22.—Percentage change in NH total column zone as a function of E.I. ($NO_x$), for two different fuel burns for the cruise altitude band of 17 to 19 km.

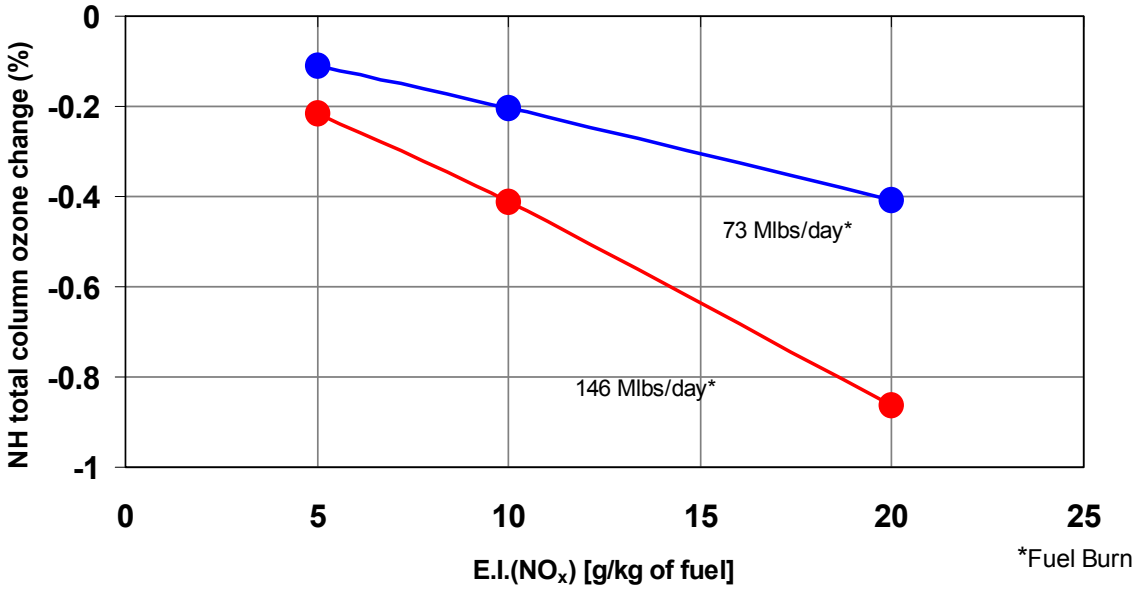


Figure 23.—Percentage change in NH total column zone as a function of E.I. ($NO_x$), for two different fuel burns for the cruise altitude band of 19 to 21 km.

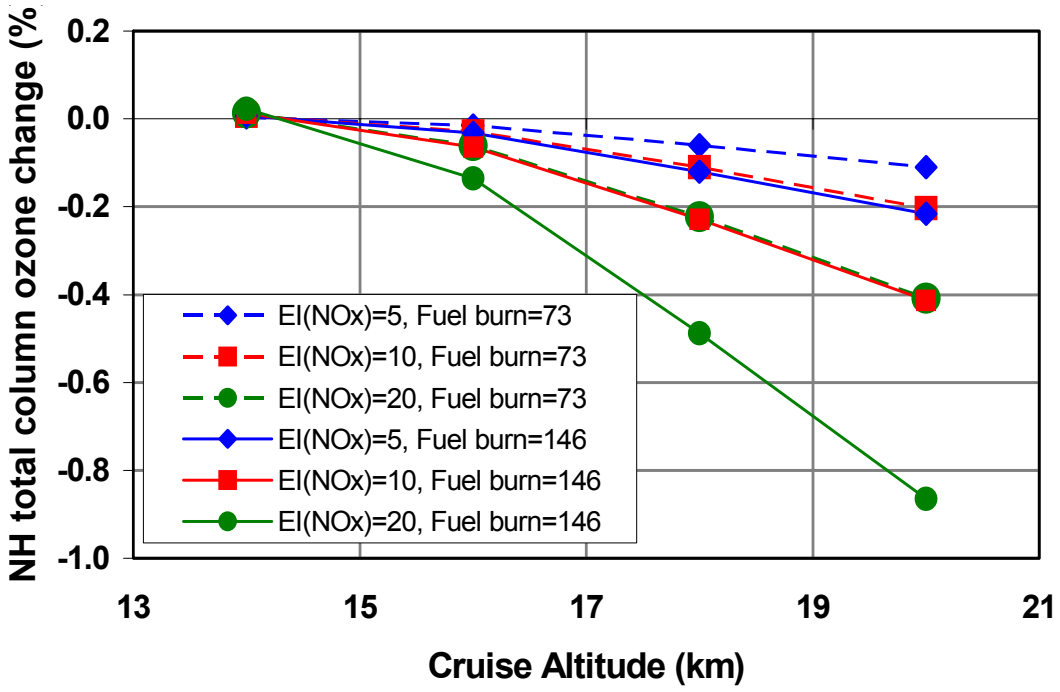


Figure 24.—Calculated column ozone impact for the Northern Hemisphere as a function of cruise altitude for different E.I. ($NO_x$) and for fuel burn of 73 Mlbs/day and 146 Mlbs/day.

Figure 24 presents the calculated column ozone impact for the Northern Hemisphere as a function of cruise altitude for different E.I. ($NO_x$) and the two fuel burn cases. In this figure the altitude sensitivity of the studies show the point in the lower atmosphere where the effect on ozone transitions from a positive effect on ozone to a negative impact. The inflexion point is near 14.25 km. Other than the lower altitude emissions cases, the cruise altitude bears a linear relationship with percentage total column ozone change.

***3.2.1. Comparison of HSCT type cases with HSCT (IPCC, 1999) cases***.—It is also valuable to compare the derived change in ozone relative to earlier scenarios and to the effect derived for subsonic aircraft fleets. Table 5 shows the effects on ozone from several scenarios for HSCT aircraft used in IPCC (1999), for the 2020-projected fleet of subsonic aircraft and for several E.I.($NO_x$) cases for the HSCT type aircraft studied in this report for the altitude range of 17–19 km. For the earlier HSCT scenarios, two of the IPCC scenarios were chosen, S1d and S1e, both of which are based on an assumed fleet of 500 HSCT aircraft but with different emission indices for $NO_x$ (IPCC, 1999). Effects on ozone from the 2020 subsonic fleet, using emissions based on Baughcum et al. (2002), was calculated in the 2–D model relative to a 2020 background atmosphere.

TABLE 5.—COMPARISON OF EFFECTS ON OZONE USING EARLIER HSCT SCENARIOS FOLLOWING IPCC (1999), HSCT SCENARIOS IN THIS STUDY AND THE 2020 SUBSONIC AIRCRAFT FLEET RELATIVE TO 2020 BACKGROUND ATMOSPHERE.

| Scenarios | Fleet Size | E.I. ($NO_x$) | Cruise Altitude | $O_3$ column change | | | $O_3$ concentration | |
|---|---|---|---|---|---|---|---|---|
| | | g/kg of fuel | km | Global | NH | SH | Max | Min |
| | | | | | | | | |
| HSCT –2015 | 500 aircraft | 10 | 17 to 20 | ------- 0.492 | ------ 0.696 | –0.288 | 0.139 | –1.823 |
| | | | | | | | | |
| | | 15 | | ------ 1.030 | ------ 1.392 | –0.667 | 0.143 | –3.822 |
| Subsonic only –2020 | ------- | -- | | | | | | |
| | | | 10.7 to 13.7 | 0.408 | 0.584 | 0.233 | 0.991 | 0.132 |
| | | | | | | | | |
| HSCT type –2020 | ~73 Mlbs/day | 5 | 17 to 19 | ------ 0.049 | ------ 0.060 | –0.038 | –0.028 | –0.154 |
| | | | | | | | | |
| | | 10 | ------- | ------ 0.086 | ------ 0.110 | –0.062 | –0.042 | –0.263 |
| | | | | | | | | |
| | | 20 | ------- | ------ 0.168 | ------ 0.222 | –0.114 | –0.035 | –0.562 |
| | | | | | | | | |
| | ~146 Mlbs/day | 5 | ------- | ------ 0.104 | ------ 0.120 | –0.088 | –0.062 | –0.332 |
| | | | | | | | | |
| | | 10 | ------- | ------ 0.183 | ------ 0.228 | –0.137 | –0.091 | –0.540 |
| | | | | | | | | |
| | | 20 | ------- | ------ 0.369 | ------ 0.487 | –0.251 | –0.052 | –1.210 |

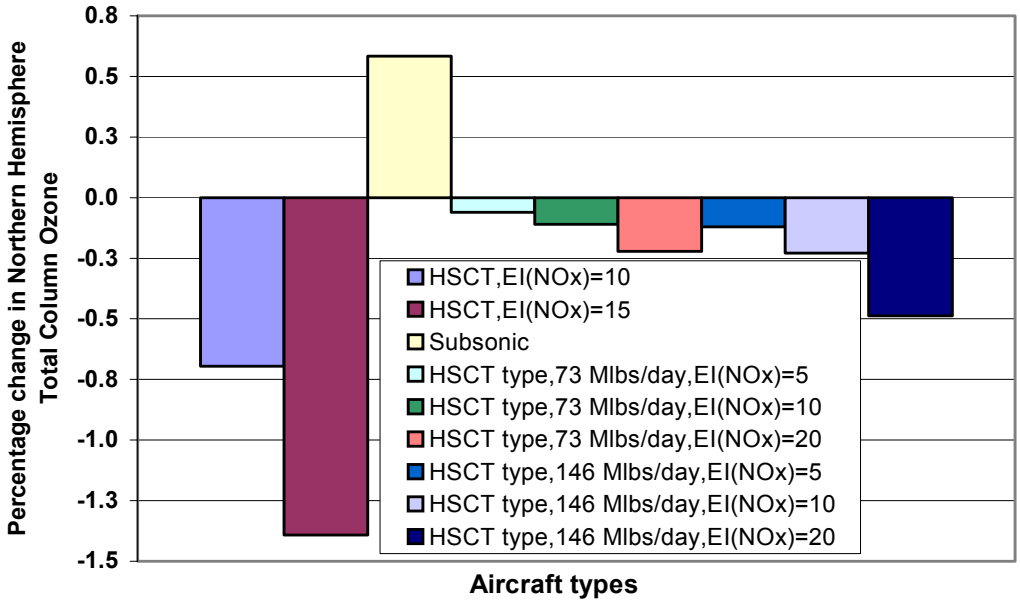


Figure 25.—Comparison of effects on Northern Hemisphere change in total column ozone for model studies of HSCT scenarios from IPCC (1999), the HSCT scenarios evaluated here, and a 2020 subsonic aircraft fleet emissions case.

Based on the results in table 5, figure 25 shows the comparative effect on Northern Hemisphere total column ozone due to the fleet of HSCT aircraft (IPCC, 1999), subsonic only aircraft and HSCT type aircraft. The effects on ozone, due to the new HSCT type aircraft is much less than the fleet of HSCT aircraft studied in IPCC (1999) report. The effect of the kind of HSCT aircraft studied in this report is at least a factor 2.5 less than the HSCT aircraft studied in IPCC (1999). The new scenarios use fuel burns that are much smaller than the scenarios used in the 1999 assessment, in recognition that a viable HSCT aircraft will need to be much more fuel efficient than the earlier designs (see Baughcum et al., 2002). The subsonic fleet produces a positive effect on total Northern Hemisphere ozone concentration.

## Conclusions

- The current version of the UIUC 2–D model generally shows much higher sensitivity than the IPCC (1999) assessment models. This overall difference is largely due to several changes in the chemistry for nitrogen oxides in the lower stratosphere, resulting in an increased sensitivity of $NO_x$ emissions on stratospheric ozone.
- The water vapor emissions have similar effects as compared to the earlier assessment analyses.
- The differences in the results for the Southern Hemisphere can be attributed to the enhancements in the treatment of dynamical processes in this version of the model, with resulting increased transport of $NO_x$ across the equatorial region.
- In this study of the potential impact of a fleet of HSCT type aircraft, the maximum local ozone depletion, even for the highest E.I. ($NO_x$) of 20 g/kg of fuel, fuel burn of 146 Mlbs/day and highest cruise altitude case, was found to be 2.22 percent. Total ozone changes in the Northern Hemisphere for this case is 0.864 percent or less.

- The maximum local ozone depletion for the more realistic scenario of a HSCT type fleet, with E.I. ($NO_x$) of about 10 gm $NO_x$ per kg fuel and cruise altitudes between 15 to 17 km, the Northern Hemisphere decrease in total ozone is equal to 0.064 percent.
- The relationship between percentage total column ozone change and E.I. ($NO_x$) is linear for all cruise altitudes.
- The relationship between percentage total column ozone change and E.I. ($NO_x$) is linear for all fuel burns as well.
- The altitude in the atmosphere above which net ozone depletion begins due to these projected flights is around 14.25 km.
- The relationship between percentage total column ozone change in the Northern Hemisphere is linear with cruise altitude for the altitude ranges above 15 km.
- This study provides crucial information for determining the optimum fuel burn, emission index of $NO_x$ and cruise altitude of the projected fleet of HSCT type aircraft, such that ozone depletion in the lower stratosphere is kept to a minimum.

## References


Arakawa, A., and W.H. Schubert, 1974: Interactions of cumulus cloud ensemble with the large-scale environment. Part I. *J. Atmos. Sci.*, 31, 671–701.

Bacmeister, J.T., D.E. Siskind, M.E. Summers, and S.D. Eckermann, 1998: Age of air in a zonally averaged two-dimensional model, *J. Geophy. Res.*, 101, 1457–1461.

Baughcum, S.L., 2002: Informal Report Describing the Development of Parametric Emission Scenarios, NAS3–01140 Revolutionary Aero-Space Engine Research Task Order #5 prepared for NASA Glenn Research Center, Cleveland, p 13.

Choi, W. 1995: On the meridional circulation in the transformed Eulerian mean system, *J. Korean. Meteor. Soc.*, 31, 325–337.

Choi, W., 1996: Eddy mixing by the planetary wave in the stratosphere. *J. Korean. Meteor. Soc.*, 32, 41–50.

Choi, W., and D. Youn, 2001: Effects of physical and numerical schemes on model-calculated ozone distribution in the stratosphere, *K. J. Atmos. Sci.*, 3, 39–52.

DeMore, W.B., S.P. Sander, D.M. Golden, R.F. Hampson, M.J. Kurylo, C.J. Howard, A.R. Ravishankara, C.E. Kolb, and M.J. Molina, 1997: *Chemical Kinetics and Photochemical Data for Use in Stratospheric Modeling*, Evaluation Number 12, Jet Propulsion Laboratory (JPL) Publication 97–4, Pasadena, California.

Dutta, M., D. Youn, K. Patten, and D. Wuebbles, A Comparison of HSCT emissions scenario results from the UIUC 2–D model with the IPCC (1999) assessment, Report prepared for NASA Glenn Research Center and The Boeing Company, Seattle, 2002, p 22.

Fleming, E.L., C.H. Jackman, R.S. Stolarski, and D.B. Considine, 1999: Simulation of stratospheric tracers using a improved empirically based two-dimensional model transport formulation, *J. Geophys. Res*., 104, 23911–23934.

Garcia, R.R. and S. Solomon, 1994: A new numerical model of the middle atmosphere, 2, Ozone and related species. *J. Geophys. Res.*, 99, 12,937–12,951.

Garcia, R.R., F. Stordal, S. Solomon, and J.T. Kiehl, 1992: A new numerical model of the middle atmosphere, 1. Dynamics and transport of tropospheric source gases. *J. Geophys. Res.*, 97, 12,967–12,991.

Gettelman, A., J.R. Holton, K.H. Rosenlof, 1997: Mass fluxes of $O_3$, $CH_4$, $N_2O$, and $CF_2Cl_2$ in the lower stratosphere calculated from observational data, *J. Geophys. Res*., 102, 19149–19159.

Hall, T.M., D.W. Waugh, K.A. Boering , and R.A. Plumb, 1999: Evaluation of transport in stratospheric models, *J. Geophys. Res*., 104, 18,815–18,839.

Hall, T.M., and R.A. Plumb, 1994: Age as a diagnostic of stratospheric transport. *J. Geophys. Res.*, 99, 1059–1069.

IPCC, 1999: Aviation and the Global Atmosphere. J.E. Penner, et al., editors, Cambridge University Press.

IPCC, 2001: Climate Change 2001: The Scientific Basis. Contribution of Working Group I to the Third Assessment Report of the Intergovernmental Panel on Climate Change [Houghton, J.T.,Y. Ding, D.J. Griggs, M. Noguer, P.J. van der Linden, X. Dai, K. Maskell, and C.A. Johnson (eds.)]. Appendix II, pp 807–816, Cambridge University Press, Cambridge, United Kingdom and New York, NY, USA, p 881.

Isaksen, I., C. Jackman, S.L. Baughcum, F. Dentener, W. Grose, P. Kasibhatla, D. Kinnison, M.K. W. Ko, J.C. McConnell, G. Pitari, D.J. Wuebbles, T. Berntsen, M. Danilin, R. Eckman, E. Fleming, M. Gauss, V. Grewe, R. Harwood, D. Jacob, H. Kelder, J.F. Muller, M. Prather, H. Rogers, R. Sausen, D. Stevenson, P. von Velthoven, M. van Weele, P. Vohralik, Y. Wang, and D. Weisenstein, 1999: Modeling the Chemical Composition of the Future Atmosphere. Chapter 4 in Intergovernmental Panel on Climate Change, Aviation and the Global Atmosphere. J.E. Penner, D.H. Lister, D.J. Griggs, D.J. Dokken, and M. McFarland (eds.), Cambridge University Press. Cambridge, UK.

Jones, D.B.A., A.E. Andrews, H.R. Schneider, and M.B. McElroy, 2001: Constraints on meridional transport in the stratosphere imposed by the mean age of air in the lower stratosphere, J. Geophy. Res., 106, 10,243–10,256.

Kawa, S.R., J.G. Anderson, S.L. Baughcum, C.A. Brock, W.H. Brune, R.C. Cohen, D.E. Kinnison, P.A. Newman, J.M. Rodriquez, R.S. Stolarski, D. Waugh, and S.C. Wofsy, 1999: *Assessment of the Effects of High–Speed Aircraft in the Stratosphere: 1998,* NASA/TM–209237, chap 4, Greenbelt, Maryland, pp 71–101.

Kim, J.K., 1999: Parameterization of land surface processes in an atmospheric general circulation model. Ph. D. Thesis, Seoul National University, p 178.

Kinnison, D.E., P.S. Connell, J.M. Rodriguez, D.A. Rotman, D.B. Considine, J. Tannahill, R. Ramaroson, P.J. Rasch, A.R. Douglass, S.L. Baughcum, L. Coy, D.W. Waugh, S.R. Kawa and M.J. Prather, 2001: The Modeling Initiative assessment model: Application to high-speed civil transport perturbation, *J. Geophys. Res*, 106, 1693–1711.

Kotamarthi,V.R., D.J Wuebbles, and R.A. Reck, 1999: Effects of nonmethane hydrocarbons on lower stratosphere and upper tropospheric chemical climatology in a two-dimensional zonal average model, *J. Geophys. Res*, 102, 3671–3682.

Langner, J., H. Rodhe, and M. Olofsson, 1990: Parameterization of Subgrid Scale Vertical Tracer Transport in a Global Two-Dimensional Model of the Troposphere, *J. Geophys. Res.*, *95*, 13691–13706.

Li, L., T.R. Nathan, and D.J. Wuebbles, 1995: Topographically forced planetary wave breaking in the stratosphere, *Geophys. Res. Lett.*, 22, 2953–2956.

Li, S., and D.W. Waugh, 1999: Sensitivity of mean age and long-lived tracers to transport parameters in a two-dimensional model, *J. Geophy. Res.*, 104, 30,559–30,569.

Manney, G.L., R. Swinbank, S.T. Massie, M.E. Gelman, A.J. Miller, R. Nagatani, A. O'Neill, R.W. Zurek, 1996: Comparison of U.K. Meteorological Office and U. S. National Meteorological Center stratospheric analysis during northern and southern winter, *J. Geophy. Res.*, 101, 10,311–10,334.

Matsuno, T., 1995: *Climate system dynamics and modeling.* Center for Climate System Research, University of Tokyo, p 341.

Nathan, T.R., E.C. Cordero, L. Li, and D.J. Wuebbles, 2000: Effects of planetary wave-breaking on the seasonal variation of total column ozone, *Geophy. Res. Lett.*, 27, 1907–1910.

Olaguer, E.P., H. Yang, and K.K. Tung, 1992: A reexamination of the radiative balance of the stratosphere, *J. Atmos. Sci.*, 49, 1242–1263.

Park, J.H., M.K. W. Ko, C.H. Jackman, R.A. Plumb, and K.H. Sage (eds.), 1999: *Models and Measurements II*. NASA Langley Research Center, Hampton, VA, p 496.

Randel, W. and R. Garcia, 1994: Application of a planetary wave breaking parameterization to stratospheric circulation statistics, *J. Atmos. Sci.*, 51, 1157–1168.

Sander, S.P., R.R. Friedl, W.B. DeMore, D.M. Golden, M.J. Kurylo, R.F. Hampson, R.E. Huie, G.K. Moortgat, A.R. Ravishankara, C.E. Kolb, and M.J. Molina, 2000: *Chemical Kinetics and Photochemical Data for Use in Stratospheric Modeling*, Supplement to Evaluation 12: Update of Key Reactions, Jet Propulsion Laboratory (JPL) Publication 00–3, Pasadena, California.

Schneider, H.R., D.B.A. Jones, and M.B. McElroy, 2000: Analysis of residual mean transport in the stratosphere 1. Model descript and comparison with satellite data, *J. Geophys. Res*., 105, 19991–20011.

Schoeberl, M.R., A.E. Roche, J.M. Russell III, D. Ortland, P.B. Hays, and J.W. Waters, 1997: An estimation of the dynamical isolation of the tropical lower stratosphere using UARS wind and trace gas observations of the quasi-biennial oscillation, *Geophy. Res. Lett.*, 24, 53–56.

Shia, R.L., M.K. W. Ko, D.K. Weisenstein, C. Scott, and J. Rodriguez, 1998: Transport between the tropical and mid-latitude lower stratosphere: Implications for ozone response to high-speed civil transport emissions, *J. Geophys. Res*. 103, 25435–25446.

Swinbank, R. and A. O'Neill, 1994: Quasi-biennial and semi-annual oscillations in equatorial wind fields constructed by data assimilation, *Geophys. Res. Lett.,* 21, 2099–2102.

Wei, C.F., S.M. Larson, K.O. Patten, and D.J. Wuebbles, 2001: Modeling of ozone reactions on aircraft-related soot in the upper troposphere and lower stratosphere, *Atmospheric Environment,* 35, 6167–6180.

Wuebbles, D.J., K. Patten, M.T. Johnson, and R. Kotamarthi, 2001: New Methodology for Ozone Depletion Potentials of short-lived compounds: n-Propyl bromide as an example, *J. Geophys. Res*., 106, 14,551–14,571.

# REPORT DOCUMENTATION PAGE

*Form Approved*
*OMB No. 0704-0188*



| 1. AGENCY USE ONLY (*Leave blank*) | 2. REPORT DATE | 3. REPORT TYPE AND DATES COVERED |
|---|---|---|
| | June 2005 | Final Contractor Report |

**4. TITLE AND SUBTITLE**

Parametric Analyses of Potential Effects on Upper Tropospheric/Lower Stratospheric Ozone Chemistry by a Future Fleet of High Speed Civil Transport (HSCT) Type Aircraft

**5. FUNDING NUMBERS**

WBS–22–714–20–25
NAS3–03091

**6. AUTHOR(S)**

Mayurakshi Dutta, Kenneth O. Patten, and Donald J. Wuebbles

**7. PERFORMING ORGANIZATION NAME(S) AND ADDRESS(ES)**

University of Illinois at Urbana-Champaign
Department of Atmospheric Sciences
Urbana, Illinois 61801

**8. PERFORMING ORGANIZATION REPORT NUMBER**

E–15134

**9. SPONSORING/MONITORING AGENCY NAME(S) AND ADDRESS(ES)**

National Aeronautics and Space Administration
Washington, DC 20546–0001

**10. SPONSORING/MONITORING AGENCY REPORT NUMBER**

NASA CR—2005–213646

**11. SUPPLEMENTARY NOTES**

Project Manager, Chowen Wey, Vehicle Systems Projects Division, NASA Glenn Research Center, organization code PRV, 216–433–8357.

**12a. DISTRIBUTION/AVAILABILITY STATEMENT**

Unclassified - Unlimited
Subject Categories: 45 and 01

Available electronically at http://gltrs.grc.nasa.gov

This publication is available from the NASA Center for AeroSpace Information, 301–621–0390.

**12b. DISTRIBUTION CODE**

**13. ABSTRACT** ***(Maximum 200 words)***

This report analyzed the potential impact of projected fleets of HSCT aircraft (currently not under development) through a series of parametric analyses that examine the envelope of potential effects on ozone over a range of total fuel burns, emission indices of nitrogen oxides, and cruise altitudes.

**14. SUBJECT TERMS**

High speed civil transport; Ozone depletion; Atmospheric impact

**15. NUMBER OF PAGES**

35

**16. PRICE CODE**

| 17. SECURITY CLASSIFICATION OF REPORT | 18. SECURITY CLASSIFICATION OF THIS PAGE | 19. SECURITY CLASSIFICATION OF ABSTRACT | 20. LIMITATION OF ABSTRACT |
|---|---|---|---|
| Unclassified | Unclassified | Unclassified | |